Government of **Western Australia**
Department of **Mines and Petroleum**

RECORD 2016/10

EVOLUTION AND DEFORMATION OF THE ONSHORE EUCLA BASIN DURING THE CENOZOIC

by
LC Mounsher

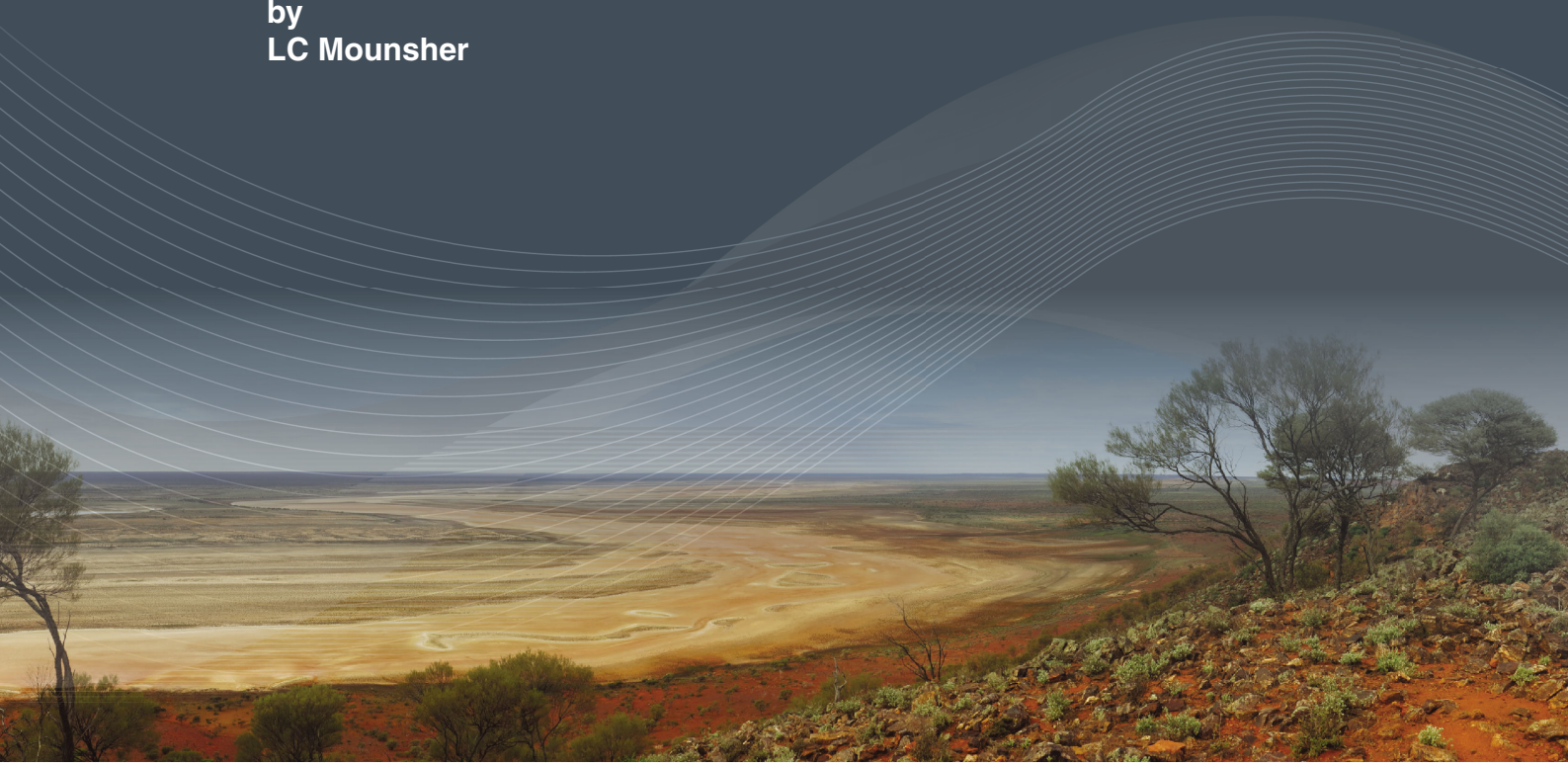

Geological Survey of Western Australia

Curtin University

Government of **Western Australia**
Department of **Mines and Petroleum**

Record 2016/10

EVOLUTION AND DEFORMATION OF THE ONSHORE EUCLA BASIN DURING THE CENOZOIC

by
LC Mounsher

Perth 2016

Geological Survey of Western Australia

REFERENCE
The recommended reference for this publication is:
Mounsher, LC 2016, Evolution and deformation of the onshore Eucla Basin during the Cenozoic: Geological Survey of Western Australia, Record 2016/10, 70p.

National Library of Australia Card Number and ISBN PDF 978-1-74168-695-1

About this publication
This Record is an Honours thesis researched, written and compiled as part of a collaborative project between the Geological Survey of Western Australia (GSWA) and Curtin University, Western Australia. Although GSWA has provided support for this project including access to core, the scientific content of the Record, and the drafting of figures, was the responsibility of the author. No editing has been undertaken by GSWA.

Published 2016 by Geological Survey of Western Australia
This Record is published in digital format (PDF) and is available online at <www.dmp.wa.gov.au/GSWApublications>.

Further details of geological products and maps produced by the Geological Survey of Western Australia are available from:
Information Centre
Department of Mines and Petroleum
100 Plain Street
EAST PERTH WESTERN AUSTRALIA 6004
Telephone: +61 8 9222 3459 Facsimile: +61 8 9222 3444
www.dmp.wa.gov.au/GSWApublications

Cover image: Elongate salt lake on the Yilgarn Craton — part of the Moore–Monger paleovalley — here viewed from the top of Wownaminya Hill, 20 km southeast of Yalgoo, Murchison Goldfields. Photograph taken by I Zibra for the Geological Survey of Western Australia

Department of Applied Geology

Honours Manuscript - 2013

Evolution and deformation of the onshore Eucla Basin during the Cenozoic

Lewis Clark Mounsher

Supervised and edited by Dr Milo Barham (Department of Applied Geology) and

Dr Michael O'Leary (Department of Environment and Agriculture)

A research project in partial fulfilment of the requirements of the unit 'Geology Honours Dissertation 400' for the degree Bachelor of Science (Honours) at Curtin University

Affirmation of Research

I hereby declare this to be a reflection of my own work. The following list details the work I took on personally in the course of completing this project:

- Field work: my supervisors and I surveyed the elevations of subsurface carbonate horizons at 27 sites (predominately caves) across the Nullarbor and Roe Plains. This was done over a period of 10 days.
- Acquisition of supplementary data: I supplemented the field data set with horizon elevations acquired from 63 drill holes. This data was sourced by sifting through 100+ online drillhole logs retained by the Geological Survey of South Australia. My supervisors and I also logged the depths of the carbonate horizons in an additional 12 Eucla Basin cores at the Carlisle Core Library.
- I created and managed a database of the field and supplementary data, and interrogated the data within Esri ArcMap and Esri Arcscene to produce 2D and 3D models as required.
- Fault analysis: I identified a number of faults on the Nullarbor and Roe Plains using a DEM and conducted various analyses on them (including the generation of displacement profiles and fault trace orientation analyses).

Lewis Mounsher

List of Contents

List of Figures

List of Tables

Abstract

The onshore component of the Eucla Basin, constituting the modern day Nullarbor and Roe Plains, has traditionally been considered a tectonically quiescent domain. However, very few studies have sought to substantiate this claim by considering the preserved evidence of onshore deformation. This study investigates the Cenozoic tectonic evolution of the onshore Eucla Basin through an examination of palaeo planation surfaces and an assessment of upper crustal faulting. A Miocene planation surface is used as a benchmark to assess the stratigraphic character of the basin, whilst the origin and nature of 46 onshore faults are speculated upon according to derived fault displacement and orientation data.

No evidence of intrabasinal warping or folding is identified in the present-day expression of the Miocene planation surface, however, an E-W elevation differential across this surface implies that the basin has undergone a degree of long-wavelength tilting. This tilting aligns with a previously described elevation differential recorded along an inboard Miocene palaeoshoreline, and accordingly, it is attributed to the dynamic topographic uplift of southwestern Australia. Analyses conducted on the suite of onshore faults suggest that they likely developed under a neotectonic compressional regime. A component of strike slip displacement or fault reactivation can be inferred from anomalously low ‘vertical displacement : scarp length’ ratios, while the coincidence of DEM lineaments and deep magnetic anomalies (indicative of fault displacement or juxtaposition of basement subcrop) implies the faults likely propagated along pre-existing crustal weaknesses. Stress field heterogeneity does not appear to have occurred across the expanse of the basin, as established by a comparison of fault characteristics either side of the centrally located (and historically significant) Mundrabilla Fault. Cumulatively, these findings describe a relatively subdued deformation history that seemingly affirms the proposed notion of tectonic quiescence.

Keywords

Eucla Basin; Nullarbor Plain; Roe Plain; Tectonics; Planation; Fault displacement

1.0 Introduction

The onshore component of the Eucla Basin is an emergent platform comprising an accumulation of Cenozoic carbonates deposited atop rift-related clastic sediments (Lowry, 1970). The present-day surface of the platform is remarkably flat, and evidence of upper crustal deformation across the region remains largely undocumented. This study seeks to broaden the understanding of Cenozoic deformation in the onshore Eucla Basin through an examination of fossil planation surfaces and an assessment of upper crustal faulting. These planation surfaces will be treated as tectonic benchmarks which, in conjunction with the faulting assessment, will shed light on the manner in which the platform evolved.

A number of factors combine to make the onshore Eucla Basin an ideal laboratory for studies assessing Cenozoic deformation. Firstly, and perhaps most importantly, the basin is geographically extensive and is characterised by the widespread development of distinctive sedimentary units. When coupled with very low erosion rates, this provides an opportunity to assess different types of upper crustal deformation operating over a range of temporal and spatial scales. Additionally, the land surface is largely devoid of vegetative cover (which readily exposes subtle landforms and outcrop), and intensive cave development across the region provides access to subsurface stratigraphy in an area with few stratigraphic drillholes (Burnett et al., 2013; Lowry, 1970).

The implications of understanding the tectonic history of the onshore Eucla Basin are varied. In a broad sense, studies of this nature have the capacity to shed light on the processes driving basin evolution on stable continental blocks. From a localised perspective, research outcomes will benefit current and future greenfields mineral exploration endeavours and hydrological studies. These findings complement the recent GSWA stratigraphic drilling program, enabling a more resolved understanding of the cover development between limited drillcore data. Furthermore, understanding the tectonic evolution of the Nullarbor Plain may improve the accuracy of palaeo-sea level estimates that are derived from the present-day elevations of ancient shorelines.

2.0 Regional Setting

The Eucla Basin lies on Australia's southern margin, bounded by the Precambrian Musgrave Province (to the north), the Gawler Craton (to the east) and the Yilgarn Craton (to the west; Fig.1; Hou et al., 2008). With spatial dimensions of ~2000 km (east-west) by ~500 km (north-south), the basin contains the most extensive onshore accumulation of Cenozoic marine

sediments recorded globally (Clarke et al., 2003). The onshore basin margins are taken as the western, northern and eastern limits of the sedimentary Eucla Group units, whilst the offshore extent is demarcated by the 200 m isobath on the continental shelf to the south (Lowry, 1970). Given its location, the development and evolution of the Eucla Basin was intimately tied to that of Australia's southern margin.

2.1 Geological evolution of Australia's southern margin

The Australian continent was adjoined to Antarctica and India from 520-180 Ma, forming the eastern edge of the Gondwana supercontinent (Johnson, 2004). The Southern Australian passive continental margin originated as a fracture in the supercontinent (McGowran, 1972), which led to rifting and subsidence during the late-Jurassic to middle-Cretaceous (Veevers, 1984). The onset of seafloor spreading between the Australian and Antarctic continents during the late-Cretaceous (Cenomanian) marked the beginning of Australia's northward drift, triggering the first incidence of marine-influenced sedimentation along the southern margin (Li et al., 2003). Continental divergence continued at slow rates (~4 mm / yr) until the middle Eocene (Veevers, 2000), when a significant increase in seafloor spreading rates widened and deepened the gulf between the two continents (O'Connell, 2011). This acceleration in spreading rates was followed by a series of marine transgressions, ultimately forming a thick succession of carbonate deposits along Australia's southern margin (Li et al., 2003; McGowran et al., 1997). As such, the sedimentary sequence of the present-day margin is typically expressed as a succession of Mesozoic terrigenous clastic sedimentary rocks, overlain by Cenozoic marine clastics and carbonates (Stagg et al., 1999).

2.2 Eucla Basin stratigraphy

Sediments of the Eucla Basin are underlain by a lithologically variable basement, comprising Precambrian granite, gneiss, schist and quartzite in the southwest, and Proterozoic sedimentary rocks in the north (Lowry, 1970; O'Connell, 2011). Siliciclastic sediments of the Loongana Formation and the conformable Madura Formation (heterolithics) were deposited directly atop the basement during Cretaceous rifting, largely concealing undulations and irregularities of the basement and forming a near-horizontal surface for the deposition of subsequent units (Lowry, 1970). With the increase in marine influence prevailing in the Cenozoic, and the resultant reduction in siliciclastic sedimentation, calcareous sandstones and limestones of the Eucla Group were deposited atop the sequence (Fig. 2; O'Connell,

2011). The onshore expression of the Eucla Group limestone succession is termed the 'Eucla Platform' (O'Connell, 2011); incorporating the Wilson Bluff Limestone, the Abrakurrie Limestone and the Nullarbor Limestone, with sediments from the later Plio-Pleistocene transgression termed the Roe Calcarenite. These units are separated by Eocene to Miocene subaerial disconformities (sequence boundaries of second and third order cycles), representing the series of marine transgressions and regressions that influenced sedimentation patterns along much of the southern margin (Li et al., 2003; O'Connell et al., 2012). The depositional extent and thickness of each of the limestones varies according to the magnitude and longevity of its corresponding transgressive event, but in spite of this, each of the units appears to retain approximate horizontality at basin-scale and displays a surprising degree of continuity across the platform (James and Bone, 2000). The limestones of the Eucla Platform represent the key stratigraphic interval for this particular study.

2.2.1 Sedimentological descriptions of the Eucla Platform limestones

The Wilson Bluff Limestone

The middle- to late-Eocene Wilson Bluff Limestone is the basal carbonate unit of the Eucla Platform. It is characteristically white, poorly-sorted, chalky and bryozoan-rich; commonly bearing whole and fragmented echinoids, bivalves, brachiopods and foraminifers (Lowry, 1970). The chalkiness has been attributed to an abundance of indeterminate skeletal fragments (Lowry, 1970), resulting in a dominance of mudstone, wackestone and packstone textures (James and Bone, 1991). The Wilson Bluff Limestone extends to the inner margin of the Eucla Platform (James and Bone, 1991), attaining a maximum (known) thickness of approximately 300 m (Lowry, 1970). It is interpreted to have been deposited on a cool to temperate continental shelf in water depths of 90 - 120 m (Lowry, 1970).

The Abrakurrie Limestone

Disconformably overlying the Wilson Bluff Limestone is the late-Oligocene to lower-Miocene Abrakurrie Limestone (Webb and James, 2006). Two broad units are recognised. The lower unit is a moderately well-sorted, thin-bedded, friable, bryozoan-rich calcarenite with foraminifera (rotalid and miliolid), bivalves, brachiopods and echinoids (Craig, 2002; Lowry, 1970; O'Connell, 2011), and commonly displays cross-bedding (Craig, 2002). The upper unit is indurated and thick-bedded, containing a notably higher abundance of echinoid tests (whole and fragmented; Craig, 2002; O'Connell, 2011). It is cyclical in nature, with hardground-capped individual cycles showing vertical gradations in grain size and faunal assemblage (O'Connell, 2011). Serpulid worms, solitary corals, gastropods and coralline algae are also present in particular regions of the upper and lower units, but are less

common than the aforementioned dominant biological constituents (James and Bone, 1991). Microbioclastic micrite commonly forms the matrix of the Abrakurrie Limestone, seemingly derived from the zooecia of cheilostome bryozoans (James and Bone, 1991). The Abrakurrie Limestone occurs in the central region of the Eucla Platform as a lens-shaped deposit (O'Connell, 2011). It attains a maximum thickness of ~90 m (Li et al., 1996), however, it has been suggested that the original depositional thickness may have been greater to the south (prior to the onset of Pleistocene marine erosion; Lowry, 1967). The Abrakurrie Limestone is interpreted to have been deposited on a shallow, open shelf (Lowry, 1970), further defined by Li et al. (1996) as a temperate-neritic environment with water depths of ~100 m.

The Nullarbor Limestone

The penultimate unit in the Cenozoic carbonate succession is the lower- to middle-Miocene Nullarbor limestone. It disconformably overlies the Abrakurrie Limestone in the central region of the platform (Webb and James, 2006), and the Wilson Bluff Limestone elsewhere (O'Connell, 2011). Two discrete members are recognised: the basal Mullamullang Member, and the conformable upper member (unofficially referred to as the Rawlinna Member).

The basal Mullamullang Member is an algal limestone comprising an accumulation of nodular lithothamnium-type coralline algae (rhodoliths) within a matrix of comminuted algae and foraminifera (Lowry, 1967). Floatstone and rudstone textures are dominant throughout the member (O'Connell, 2011), and the abundance of rhodoliths gives the rock a distinctive pink colouration on unweathered surfaces (O'Connell et al., 2012). The Mullamullang Member of the Nullarbor Limestone represents a basal biostrome that underlies the more diverse upper member, with a comparatively restricted distribution. It thickens southward from its depocentre (the town of Madura), attaining a maximum thickness of approximately 10 m along the Hampton Range (Lowry, 1967). It is interpreted to represent a transgressive rhodolith gravel deposit, typical of those that form in the lower photic zone (15 – 30 m) in mesotrophic waters (O'Connell et al., 2012).

The upper member of the Nullarbor Limestone is, by comparison, lithologically diverse and highly fossiliferous (O'Connell, 2011). The faunal assemblage of the unit is dominated by fragmented echinoids, foraminifers (benthic and planktonic) and coralline algae, but also contains bivalves, gastropods, serpulid worm tubes, bryozoans and scleractinian corals (Lowry, 1967; O'Connell et al., 2012). Many skeletal grains display micrite envelopes under magnification, and moldic preservation, particularly of bivalves and gastropods, is common (Lowry, 1967). Textures range from mudstones to rudstones across the basin (James and Bone, 1991), and the unit is generally well-cemented and devoid of sedimentary structures (O'Connell, 2011). The Nullarbor Limestone upper member was deposited extensively across

the Eucla Platform, covering approximately 120,000 km^2 of the present-day plateau surface (O'Connell, 2011). Although its maximum depositional thickness is indeterminate (given the effects of post-Miocene subaerial and submarine erosion), drillhole logs suggest that it exceeds 50 m in parts. The upper member of the Nullarbor Limestone grades laterally into the calcareous Colville Sandstone inboard, and is considered to represent widespread shallow marine deposition (O'Connell, 2011). Lowry (1970) proposed that the unit was deposited across a broad, open shelf that was characterized by good circulation, normal marine salinities and water depths in the range of 30 – 45 m.

The Roe Calcarenite

The youngest limestone deposited on the Eucla Platform, the Roe Calcarenite, veneers the Roe Plain; a marine erosional surface that was cut into the centre of the Great Australian Bight during the late-Pliocene to early-Pleistocene (James and Bone, 2007). The calcarenite is weakly lithified, coarse-grained, poorly-bedded and highly fossiliferous (Lowry, 1970). The macro-faunal assemblage is dominated by molluscs (a diverse range of bivalves and gastropods), echinoids, large benthic foraminifera and coralline algae (James and Bone, 2007). The finer-grained fraction of the rock comprises fragmented particles of echinoids, foraminifera, serpulid worm tubes, molluscs and coralline algae (James and Bone, 2007). Detrital clasts (including quartz grains, intraclasts and lithic fragments) typically constitute 10-15% of the rock (James and Bone, 2007). Minor micrite occurs around bioclasts (Lowry, 1970), and the commonly occurring textures are rudstones, grainstones and floatstones (James and Bone, 2007). The Roe Calcarenite was deposited relatively uniformly across the Roe plain, covering approximately 8,000 km^2 at a thickness of 2-3 m (James and Bone, 2007; Lowry, 1970). It disconformably overlies the Wilson Bluff Limestone in the eastern parts of the Roe Plain, and the Abrakurrie Limestone elsewhere (Lowry, 1970). The calcarenite has been broadly interpreted as a product of shallow marine, subtidal sedimentation in a seagrass-dominated environment (James and Bone, 2007). The composition of the faunal assemblage suggests that the shallow marine setting in which the calcarenite accumulated was at least periodically influenced by tidal currents and/or open ocean swell (James et al., 2006).

2.3 An overview of Cenozoic tectonics in the onshore Eucla Basin

The Nullarbor Plain has traditionally been considered a tectonically quiescent domain (Hillis et al., 2008), with very few early studies considering the onshore evidence of Cenozoic tectonic activity. In an extensive study of the Eucla Basin geology, Lowry (1970) made some preliminary, yet important observations regarding local tectonic features. A northward

trending fault lying immediately north of the town of Madura was recognised as having a significant amount of vertical displacement. Based on field observations, Lowry inferred that this structure was associated with apparent folding to the south. Another substantial fault approximately 25 km NNW of Caiguna was correlated with a geophysical gravity anomaly, with the resultant assessment of the data revealing that the fault plane was likely very steep (dipping at approximately 89° to the west). Given the linearity of the fault scarps identified at the time, and the traditional inference of relative tectonic quiescence, Lowry postulated that the faults were most likely to have a normal sense of displacement.

More recently, the tectonic history of the onshore Eucla Basin has received greater attention from the scientific community. Studies of Australian 'neotectonic' deformation (defined as deformation that occurred under the current crustal stress regime) have reviewed faulting on the Nullarbor Plain as a means of investigating intraplate deformation in stable continental regions. Clark et al. (2012) recognised a large number of previously unidentified faults in the Nullarbor region via a digital elevation model, concluding that maximum vertical displacements had not exceeded a few tens of metres over the last 15 million years. This corresponds to average neotectonic slip rates of 1-3 m Ma^{-1}; values that have been said to reflect the continuing tectonic stability of the local Proterozoic basement (Clark et al., 2012). Given the shortage of local stress field data from the Nullarbor region, and the approximately N-S orientation of many of the fault scarps being scrutinised, it has been proposed that this deformation occurred in response to the regional-scale, E-W oriented maximum horizontal stress that has been inferred from plate boundary force modelling (Hillis et al., 2008). Current research has also highlighted the tectonic significance of one particular fault, the Mundrabilla Fault, which occurs in the south-central region of the Nullarbor Plain. Although this fault initially appears to be a localised feature on the Plain, it is thought to correlate with the N-S trending, continent-scale Lasseter Shear Zone (Fig. 3; D'Ercole and Lockwood, 2003). Whilst the current research effort is largely focused on large-scale Precambrian motions on the shear, it has been suggested that the Mundrabilla Fault is lithospheric-scale and it may be sustaining a large differential stress (A Aitken 2013, pers. comm., 11 Sep.).

The Eucla Basin has also yielded important evidence of continent-scale Cenozoic crustal deformation. Sandiford (2007) noted a distinct latitudinal asymmetry in the geomorphology of the Australian landmass, expressed through a number of irregularities in the sedimentary record. The continental shelf along Australia's southern margin is characteristically 20 – 200 km wide. Onshore, Cenozoic marine sediments have been preserved up to 250 m above the present-day sea level. In contrast, the continental shelf along Australia's northern margin is typically 200 – 500 km in width, with Cenozoic marine sediments lying almost exclusively below present-day sea level. When the eustatic signal is eliminated, this data implies that

significant continent-scale tilting transpired throughout the Cenozoic (SW up, NNE down), generating a total differential vertical displacement of as much as 300 m over the last 15 million years (Sandiford, 2007). This apparent uplift of the south western region of the continent is also evidenced by variability in the present-day elevations of coeval (early Neogene) palaeoshorelines, which decrease eastward by approximately 150 m over a 760 km interval in the onshore Eucla Basin (Quigley et al., 2010; Sandiford, 2007). The primary mechanism believed to be responsible for this long-wavelength (10^3 km) tilting is dynamic topography - defined as upper crustal deflection in response to differential mantle buoyancy patterns (Quigley et al., 2010). Zones of mantle downwelling are manifested at the earth's surface as topographic lows, and upwellings tend to produce topographic highs (Sandiford, 2007). For 15 million years the Australian continent has been steadily drifting away from a significant zone of mantle downwelling that lies to the south (as evidenced by the Australian-Antarctic Discordance), while simultaneously, the northern margin has been drifting towards a dynamic topographic low defined by the Indonesian subduction zone (Sandiford, 2007). The theoretical result of this drift path would be subsidence of the northern margin and emergence of the southern margin, as has been inferred from the sedimentary record.

3.0 Materials and Methods

Cenozoic tectonism in the Eucla Basin was assessed in two phases. The first phase involved the acquisition, analysis and modelling of a data set representing the present-day elevations of key subsurface lithostratigraphic contacts at a number of sites across the Nullarbor and Roe Plains. These horizons represent fossil planation surfaces and, as such, an evaluation of their present-day character can potentially highlight any local or regional-scale Cenozoic deformation that prevailed on the platform. In the subsequent phase of the study, faults expressed on the surface of the plains were analysed through the interrogation of a high resolution digital elevation model. This characterisation of regional faulting was important in the context of elucidating poorly-defined local stress regimes, and developing an understanding of the rate at which brittle deformation has modified the platform.

3.1 Acquisition of contact elevation data

The basal Abrakurrie Limestone horizon (i.e. Wilson Bluff – Abrakurrie Limestone contact), the basal Nullarbor Limestone horizon (composite surface comprising the coeval 'Abrakurrie – Nullarbor Limestone' and 'Wilson Bluff – Nullarbor Limestone' contacts) and the basal Roe

Calcarenite horizon (composite surface encompassing the 'Abrakurrie – Roe Calcarenite' and the 'Wilson Bluff – Roe Calcarenite' contacts) are all thought to have approximated horizontal surfaces at the time of their formation. The use of these stratigraphic horizons as tectonic benchmarks is justifiable according to the mode of formation of the Eucla Platform. As previously alluded to, the deposition of Cretaceous clastic sediments in the Eucla Basin largely neutralised topographic undulations and irregularities in the basement surface, thereby generating a relatively flat foundation for the deposition of the Cenozoic limestones (Lowry, 1970). James and Bone (2000) acknowledged the high degree of basin-scale horizontality exhibited by these limestones; a fact that is substantiated by the extremely shallow present day N-S slopes of the Nullarbor Plain (0.02°), the Roe Plains (0.01°) and the Great Australian Bight sea floor (0.02°). It has also been noted that each of the Eucla Platform limestones was deposited during a discrete transgressive event. As such, it is postulated that marine planation would have immediately preceded the deposition of each limestone, further levelling the upper surface of the underlying unit. Whilst localised palaeotopographic and/or karstic features may prevail in certain areas, approximate horizontality of the planation surfaces would be expected to predominate at a kilometre-scale. Thus, visualisation of the present-day character of these originally planar horizons should yield evidence of significant post-depositional tectonic deformation.

3.1.1 Field data acquisition

A total of 27 field sites were selected on the Nullarbor and Roe Plains. The suite of sites comprised 19 caves/rockholes, three road cuts, two coastal outcrops, two gullies along the Hampton Escarpment and one quarry. Horizons were constrained at each site based on the sedimentological parameters of the bounding limestones, and elevations were measured to a high degree of accuracy (+/- 15cm) through the use of a differential GPS and a laser total station (methodology is outlined in Appendix 1). Sedimentological data were also recorded at each field site (Appendix 2). All horizons were examined for evidence of karstification, erosion or irregular depositional topography. These records represented a means by which excessive or anomalous local variability in contact elevations could be investigated.

3.1.2 Supplementary data acquisition

Given the vast geographic extent of the Eucla Platform, it was advantageous to supplement the field data set with additional elevation data. Supplementary data was sourced from online drilling records (from the South Australian Geological Survey), published literature and

drilling chips. In each case, the logged contact depths were converted to elevations using DEM values taken at each site. Figure 4 depicts the locations of the field sites, and the sites from which supplementary elevation data was obtained.

Online drilling records

Elevation data for an additional 63 sites were acquired through an extensive review of online drilling logs supplied by the Geological Survey of South Australia. The 'basal Nullarbor Limestone' horizon was the benchmark horizon that had been intersected in each of these drill holes.

Published literature

Lowry (1970) produced stratigraphic logs for 18 sites on the Nullarbor Plain. Although elevations were determined using comparatively simplistic equipment (an aneroid altimeter), Lowry's technique enabled him to log deep stratigraphic sections in caves where a high degree of passage tortuosity precluded the use of the laser sighting system. As such, numerous contact elevations that were not able to be accurately measured in the field were adapted from Lowry's work and incorporated into the data set.

Drilling chips

The final set of supplementary elevation data was acquired through the logging of RC drilling chips retained by the Geological Survey of Western Australia. Twelve drill holes were logged, providing contact elevation data for the central to northern regions of the Nullarbor Plain.

3.1.3 Analysis and visualisation of contact elevation data

Following the conversion of all elevations to the Australian Height Datum (representing elevations above mean sea level), the complete contact elevation data set was stored, interrogated and analysed within ESRI ArcMap10. This facilitated visualisation and interpretation of the data in the context of a digital elevation model and regional geological maps. Additionally, the benchmark horizons were able to be modelled as two-dimensional colour-contoured raster images, providing simple representations of the present-day character of these originally planar surfaces. To further assist with data interpretation, the digital elevation model and the horizon raster images were also modelled in three dimensions within ESRI ArcScene10.

3.2 Fault analyses

A total of 46 faults on the surface of the Nullarbor and Roe Plains were identified through the interrogation of a high resolution (shuttle radar topography mission [SRTM] 30 m) digital elevation model (Fig. 5). Displacement profiles were generated for the 27 faults that were deemed significant (with respect to their apparent vertical displacement or fault scarp length), in order to investigate fault displacement patterns across the Eucla Platform. Additionally, an analysis of fault trace orientations was conducted for the entire suite of faults for the purpose of making inferences with respect to the local vs. regional stress regimes. All fault data was then reviewed in the context of available magnetic geophysical data.

3.2.1. Generation of displacement profiles

In the absence of reliable offset markers through which strike slip movement could be quantified, vertical displacement profiles were generated to assess surficial throws on faults across the region. These displacement profiles were created using the following methodology. First, land surface elevation profiles were generated for the up-thrown and down-thrown side of each fault. This was achieved through the application of Esri ArcMap profiling operations to the digital elevation model, with data acquired at 100 m intervals along each fault trace. Fault throws (calculated as the difference between corresponding data points on the up-thrown and down-thrown sides) were then plotted against distance along the trace of the fault scarp.

The effects of modern karstification has degraded the elevation of the present day land surface by up to 5 m with short-wavelength, quasi-random variability. Therefore, where more recent geomorphological features could be discounted, the maximum elevation of a surface (typically representing outcrop) were assumed to represent the pre-karst elevation of the surface. The effects of inferred karstification on the displacement profiles were nullified through the addition of trend lines from these highs. These trend lines were manually applied so as to honour long-wavelength displacement patterns whilst adhering to the peak displacement values preserved along each fault scarp (Appendix 3). However, it should be noted that weathering and erosion of fault scarps, reducing the immediate apparent displacement of the land-surface, is difficult to constrain. Whilst Clark et al. (2012) had previously provided collective displacement estimates for the suite of faults on the Nullarbor and Roe Plains, implementation of the more robust methodology (outlined above), on a more detailed DEM was deemed worthwhile for the purpose of investigating individual fault

displacement parameters and resolving finer displacements on smaller faults, and especially at fault tips.

3.2.2. Analysis of fault orientations

The orientation of the surface traces were also measured for all of the faults identified on the Nullarbor and Roe Plains. Multiple trend values were recorded for individual faults where non-linear fault traces could be clearly subdivided into discrete segments of differing orientation. The orientation data were then plotted on rose diagrams (10° bin intervals) such that regional patterns could be identified.

3.2.3 Review of magnetic data

Regional aeromagnetic data was reviewed within Esri ArcGIS for the purpose of further characterising the Nullarbor and Roe Plains faults. By overlaying the fault traces on the geophysical data, the faults were able to be classified as potential near surface faults (those lacking a corresponding gravity or magnetic anomaly) or deeper faults (those represented in the geophysical data).

4.0 Data

4.1 Field data evidencing marine planation

Observational and quantitative data collected in the field strongly support the marine planation premise that is central to this study. Inspection of the lithostratigraphic boundaries across the field study area revealed an insignificant degree of local palaeokarstic variability, essentially nullifying the notion that karst processes might have significantly impacted contact horizontality on a local scale. Palaeokarstic irregularities never exceeded ~10 cm along any given contact (Fig. 6); even where extensive outcrop exposed contacts over relatively long distances (e.g. the basal Nullarbor Limestone horizon is exposed continuously for over 200 m at the Madura road cut). Data evidencing the horizontality of the planated limestone surfaces was also collected at the Madura Quarry on the Roe Plain. Here, removal of the largely unlithified Roe Calcarenite (the Plio-Pleistocene unit that veneers the surface of the Roe Plain) has exposed the planation surface that developed on the underlying, indurated Abrakurrie Limestone > 2 million years ago. Elevation data were acquired at 75 points across

the quarry floor (i.e., the planation surface) over an area of 130,000 m^2. Analysis of the data revealed a maximum elevation differential of only 57 cm across the quarry (values ranged from 17.247 m to 17.816 m ASL), exemplifying the effectiveness of marine planation in generating 'locally planar' erosional surfaces (Fig. 7).

4.2 Contact elevation data

Despite the acquisition of a large number of data points representing a broad distribution of field sites and drill holes, data density issues hampered modelling of the basal Abrakurrie Limestone and basal Roe Calcarenite horizons (raw data is provided in Appendix 4). The shortage of data representing these horizons reflects the inaccessibility of the deeper basal Abrakurrie contact in many caves, and the relative scarcity of exposures of the basal Roe Calcarenite contact. The basal Nullarbor Limestone horizon, however, could be confidently modelled over a large area of the platform (Fig. 8). On a regional scale, the modelled horizon demonstrates a notable degree of tilting- seemingly about a NE-SW axis. Elevations in the south east are typically less than 30 m ASL (and locally as low as 9 m), whilst the horizon reaches a peak elevation of 180 m ASL approximately 400 km to the northwest. This corresponds to a maximum slope of 0.02°. Localised perturbations of the otherwise uniform slope are evident immediately north of the Roe Plain, and toward the eastern margin of the Nullarbor Plain.

4.3 Fault data

Profiles generated for the selected faults reveal maximum vertical displacements between 11.9 m and 33.9 m (with a mean value of 18.8 m; Fig. 9). Scarp lengths over which these displacements accumulated range from 21 km to 203 km. The profiles exhibit a variety of displacement distribution patterns; including 'peak type', 'bell-shaped' and 'plateau' distributions (Fossen, 2010). Fault trace orientation data for the entire suite of faults (split into discrete fault segments, defined by orientation and displacement magnitude, as necessary) are presented in figure 10. The majority of faults trend between 340° and 060°. The fault trace orientation distribution is bimodal, with modal strike intervals at 340° – 010° (n = 41 faults / fault segments) and 030° – 050° (26 faults / fault segments).

Magnetic data representing the study area shows that the majority of faults selected for the displacement profile analysis (i.e. those demarcated in black) have a corresponding magnetic signature (Fig. 11). Interestingly, many of the smaller faults with comparatively

insignificant surface expressions (demarcated in red) also track deep magnetic anomalies. Although the strength and nature of each signature varies, surface expressions of faulting were not found to be noticeably or consistently offset from their associated geophysical signatures. A summary of fault characteristics is provided in Table 1.

5.0 Data Interpretation

5.1 Character of the basal Nullarbor Limestone horizon

Over the geographic range of the data set, the present-day expression of the basal Nullarbor Limestone horizon is strikingly similar to that of the modern Eucla platform surface. The 0.02° (maximum) palaeo-slope of the horizon, as measured over a SE-NW transect, actually matches the corresponding slope of the modern platform perfectly. Therefore, assuming continuity and uniformity of local karstic and erosional processes between the Miocene and the present, it is proposed that the basal Nullarbor Limestone planation surface has broadly retained the character of the lower Miocene palaeo-platform (i.e. no large-scale internal warping or folding of the surface is apparent). The tilting of the horizon about a NE-SW axis, which is equally evident on the modern platform surface, was likely generated by long-wavelength E-W deflection of an originally southward-sloping ramp. This sense of deflection parallels the palaeoshoreline elevation differentials defined by Quigley et al. (2010) and Sandiford (2007), and as such, it may serve as a useful constraint for further characterisation of long wavelength dynamic topographic uplift (refer to section 6.1).

The localised perturbations of the otherwise uniformly sloping basal Nullarbor Limestone horizon, noted in section 4.2, occur immediately adjacent to faults 9 and 16. These anomalies simply reflect vertical displacements along the faults that have had a disproportionate influence on the character of the horizon due to the distribution of proximal data points. To overcome this bias, and to impartially assess the regional impact of localised faulting, relative displacements across all significant faults were subsequently ‘forced’ into the basal Nullarbor Limestone model (Fig. 12). This was achieved by incorporating a number of pseudo-data points into the model (flanking each of the major faults) that imposed surficial fault offsets onto the subsurface horizon. The net result demonstrates satisfactorily that fault systems across the platform do not have a perceptible influence on the broad stratigraphic character of the basin (i.e. the effects of fault offsets are relatively localised). Given the indication of long-wavelength E-W tilting, and the relative internal homogeneity of the modelled horizon, it is suggested that the Eucla Platform behaved as a rigid and coherent body during its most recent emergent phase.

5.2 Interpretation of fault data

An examination of the fault displacement profiles facilitates the estimation of fault growth rates on both the Nullarbor and Roe Plains. For the purpose of Nullarbor Plain fault growth calculations, it is assumed that the development of the surficial Nullarbor Limestone (and that of its coeval inboard equivalent) ceased 15 million years ago. Similarly, Roe Plains fault growth rates are calculated under the assumption that the development of the Roe Calcarenite halted 2 million years ago. In each case, displacement is taken to have accumulated post-depositionally. Under these assumptions, the maximum displacement identified on a Nullarbor Plain fault (33.9 m; fault number 19) corresponds to a vertical displacement rate of 2.26 $m.Ma^{-1}$. The Nullarbor fault accommodating the lowest maximum surficial displacement (fault 18; 12.6 m) yields a vertical displacement rate of 0.84 $m.Ma^{-1}$. By contrast, the maximum displacement observed on the surface of the ~2 million year old Roe Plains is 13.4 m (fault nine), corresponding to a significantly higher displacement rate of 6.7 $m.Ma^{-1}$. Fault 10, the only other fault cross-cutting the Roe Plains surface, accumulated displacement at a rate of 5.95 $m.Ma^{-1}$.

The robustness of the displacement estimates derived for faults on the Nullarbor Plain was tested through a spatial comparison of surface-apparent fault displacement magnitudes vs. rainfall isohyets and local (surface) geology. As the magnitude of displacement values showed no correlation with either parameter, it can be assumed that neither rainfall variability nor differences in the composition of different lithological units affected the weathering or erosion susceptibility and the apparent derived displacement estimates. It should be noted, however, that the standardised methodology used to apply trend lines to the displacement profiles (Appendix 3) may have produced slightly inflated maximum displacement estimates for faults on the Roe Plain. This would be anticipated due to the lesser degree of karstification of the younger plain, and undulations of more recent geomorphological features such as dunes on the Roe Plains not being relevant to fault displacement magnitudes.

The faults identified across the platform are likely to have developed under a relatively consistent stress regime, as indicated by the clustering of strike values depicted on the rose diagram (Fig. 10). Magnetic signatures associated with many of the faults could be taken as evidence for the penetrative depth of crustal strain across the region, or may even imply that deeper, pre-existing structures were reactivated during the past 15 million years. Given the thickness of the pure carbonate succession, these signatures would likely be indicative of continued displacement at depths greater than 400 m. The lack of offset between surface ruptures and their corresponding magnetic anomalies implies that fault planes are

approximately vertical. In light of this fact, the vertical fault offsets measured at the land surface can be considered a good approximation of dip slip displacement.

6.0 Discussion

To develop a broader understanding of the Eucla Platform's tectonic history, data pertaining to the basal Nullarbor Limestone horizon and the suite of onshore faults will be considered in the context of a number of pertinent factors. The tilt of the horizon will be discussed in light of previously established evidence for long-wavelength dynamic topographic uplift, and the relationship between onshore faulting and the neotectonic stress field will be examined. Fault kinematics, growth rates and growth models will then be reviewed; focusing on the evidence available to support different deformation models for the platform. Finally, the influence of the somewhat significant Mundrabilla Fault on the prevailing stress regime will be assessed.

6.1 The basal Nullarbor Limestone horizon – constraints on tilting

Quigley et al. (2010) and Sandiford (2007) alluded to middle-Miocene palaeoshoreline elevation differentials in the onshore Eucla Basin as evidence for the E-W component of continent-scale 'SW-up, NNE-down' tilting. A comparison of the degree of tilting apparent in the ~15 Ma palaeoshoreline with that of the ~16.5 Ma basal Nullarbor Limestone horizon will therefore provide an additional constraint on the magnitude and timing of this long-wavelength deformation. Sandiford (2007) noted that the elevation of the middle-Miocene palaeoshoreline decreased eastward by 150 m over a distance of 760 km. By comparison, the elevation differential recorded across a 400 km-long parallel transect on the basal Nullarbor Limestone horizon was approximately 160 m (transect locations are depicted in figure 13). Given the orientation of the transect relative to the inferred palaeo-slope, a component of the 160 m elevation differential recorded along this surface will be attributable to the palaeo-slope itself. The removal of the palaeo-slope component (in this case, 85 m) from the original 160 m elevation differential yields a 75 m residual; representative of the eastward decrease in elevation across 400 km of the basal Nullarbor Limestone horizon. This corresponds to an E-W tilt angle of 0.01° for the horizon, which is indistinguishable from the tilt defined by the palaeoshoreline data. As such, the tilting exhibited by the basal Nullarbor Limestone horizon clearly supports the notion of dynamic topographic uplift described by Quigley et al. (2010) and Sandiford (2007).

Interestingly, facies associations across the platform may imply a degree of pre-existing tilting at the onset of lower- to middle-Miocene carbonate sedimentation. In a comparison of time-equivalent sections of the upper Nullarbor Limestone, O'Connell (2011) identified deepwater planktonic foraminiferal facies in the eastern region of the platform and coeval upper photic zone benthic foraminiferal facies in the west. This significant difference in interpreted depositional depths across the platform is unlikely to have been generated during the ~1.5 million year depositional period of the Nullarbor Limestone and, as such, it advocates an earlier onset of E-W tilting than the 15 Ma value provided elsewhere.

6.2 Localised faulting and the stress field

It has been suggested that ongoing intraplate deformation is largely a function of far-field stresses associated with plate boundary interactions (Clark et al., 2012; Hillis et al., 2008; Quigley et al., 2010). The manifestation of these stresses across the Australian continent gives rise to the neotectonic stress field, which provides a basis for the interpretation of suspected neotectonic structures. The Eucla Platform faulting will therefore be considered in the context of the neotectonic stress field (on both a continent scale and a local scale), to potentially provide a better understanding of the nature of the observed deformation.

6.2.1 The continent-scale neotectonic stress field

The Australian neotectonic stress field, as defined by maximum horizontal stress directions, is somewhat anomalous. Unlike the prevailing stress field of many other continental regions (such as Europe and the Americas), the Australian stress field is not simply aligned parallel to the direction of overall plate motion (Hillis et al., 2008; Quigley et al., 2010). Rather, it is a latitudinally and longitudinally variable field that has been attributed to a complex and evolving suite of interactions along the boundary of the Indo-Australian Plate (Hillis et al., 2008). Figure 14 depicts a broad interpretation of the neotectonic stress field, as defined by the dominant maximum horizontal stress direction (σ_{Hmax}) across the continent (Hillis et al., 2008). This broad-scale model indicates that σ_{Hmax} is oriented approximately E-W across the Eucla Basin which, on the simplest level, would suggest that the ~N-S striking suite of Eucla Platform faults might share a neotectonic origin under a compressional stress regime. This notion is also supported by a number of similarities between the local faults and known neotectonic ruptures to the west; including the lack of an association with historic seismicity and comparatively small vertical displacements (Clark et al., 2012).

Further inferences pertaining to local faulting can be made according to continent-scale stress field patterns. Much of Australia's neotectonic activity is concentrated along narrow zones that are oriented normal to the regional σ_{Hmax} direction (Hillis et al., 2008). This relationship predicts relative neotectonic quiescence for the Eucla Basin region, which parallels the E-W compressive stress. Accordingly, it has been suggested that neotectonic deformation in areas such as the Eucla Basin would be characterised by the reactivation of inherited zones of weakness (faults or shears) that are preferentially aligned with the prevailing stress field (Hillis et al., 2008).

6.2.2 The local neotectonic stress field

Whilst the implied E-W regional orientation of σ_{Hmax} could plausibly explain the N-S trend of localised faulting on the Nullarbor, the character of the local stress field should still be explored. As the majority of data contributing to stress field models are derived from the study of petroleum wells or seismic events, there is no onshore data representing the Eucla Platform itself. However, stress data collected at a number of localities surrounding the Nullarbor region indicate a highly complex local stress regime (Fig. 15). Onshore, E-W to NE-SW oriented maximum horizontal stresses have been associated with strike slip tectonics either side of the Eucla Basin (in the Flinders Ranges to the east, and the Yilgarn Craton to the west; Hillis et al., 2008). Similarly oriented maximum horizontal stress vectors have also been recorded in extensional and compressional regimes (to the west and the east respectively). Offshore data in the Great Australian Bight reveals that the maximum horizontal stress direction crudely parallels the coastline, although the stress regimes associated with these data points were indeterminate. Two data points due south of the Roe Plains represent a notable exception to this coastline-parallel pattern, seemingly implying a coastline-perpendicular (N-S oriented) σ_{Hmax} direction. These data points broadly align with the onshore, N-S striking Mundrabilla Fault (Lasseter Shear Zone), which is now known to have an Antarctic counterpart associated with significant subglacial topography (A Aitken 2013, pers. comm., 11 Sep.). Given the comparatively restricted development of the Mundrabilla Fault on the southern edge of the Nullarbor Plain (in spite of the extensive northward continuity of the underlying shear), the perturbation of the stress field south of the Roe Plains may signify a neotectonic reactivation of the southern section of the Lasseter Shear Zone. If this has indeed occurred, the absence of the Mundrabilla Fault on the Roe Plains surface may indicate that the reactivation halted approximately 2 million years ago.

6.3 Fault kinematics, growth rates and growth models

6.3.1 Kinematics

As described in section 6.2.1, the orientation of the regional stress field would imply a dominance of compressional structures on a series of N-S striking faults. However, unequivocally demonstrating a reverse sense of dip-slip displacement is difficult in light of the vertical orientation of fault planes and the lack of onshore seismic data. Extensive subaerial mass wasting and erosion on the surface of the platform has effectively obscured the true orientation of the high-angle fault planes, instead producing a generic surface expression that would appear to represent extensional faulting. Consideration of the topographic profiles across localised fault systems also fails to provide an unambiguous interpretation of fault kinematics, as the resultant profiles exhibit geometries that could plausibly be generated in either an extensional or compressional regime. The fault system comprising faults 7, 8, 9 and 11 serves as a good example, wherein the topography generated across the system by the respective fault offsets could conceivably represent either a 'horst and half graben' system, or a high-angle reverse system bearing a central pop-up block (Fig. 16). According to Hillis et al. (2008), every Australian case of Quaternary onshore faulting has been characterised by reverse dip slip, or reverse-dominated oblique-slip displacement. Under this premise, it could be implied that fault nine is indeed a high angle reverse fault (as per its Quaternary expression on the Plio-Pleistocene Roe Plain). This hypothetical notion would support the 'high angle reverse pop-up block' model for the fault system depicted in figure 16 (d).

Despite the ambiguity surrounding the sense of dip slip displacement, it should also be acknowledged that evidence exists in support of strike slip deformation on the Eucla Platform. Neotectonic strike-slip movement could arguably be inferred from the fault growth patterns (Fig. 17). In a predominately dip slip regime, fault growth dynamics would suggest that the maximum vertical displacement (d_{max}) recorded along any fault would increase proportionally with scarp length (L) (Cowie and Scholz, 1992; Walsh and Watterson, 1988). This relationship is somewhat apparent in the shorter Eucla Platform faults (i.e., those having scarp lengths less than ~65 m), however, the longer faults on the platform are characterised by anomalously low vertical displacement values. A degree of strike slip motion on the longer faults would be one possible explanation for this phenomenon. Interestingly, no indication of strike slip movement is apparent where faults 9, 12 and the Mundrabilla Fault intersect the Hampton Scarp (the 2 Ma palaeo-sea cliff). This may imply that any such displacement has waned over the last 2 million years, however, the rather low growth rates on these faults might preclude the identification of correspondingly small strike slip offsets via satellite imagery.

Whilst the anomalous 'd_{max} : L' ratios could feasibly indicate strike slip displacement, they could also be rationalised in the context of fault reactivation. As discussed in section 6.2.1, the orientation of the platform with respect to the regional σ_{Hmax} direction may give rise to a predisposition to fault reactivation where pre-existing zones of weakness are sympathetically oriented. In a review of fault growth characteristics, Kim and Sanderson (2005) studied the 'd_{max} : L' ratio for a number of reverse reactivated faults (i.e. faults that were generated under a particular stress regime and later reactivated under a contrasting regime). It was deemed that such faults could also exhibit anomalously low 'd_{max} : L' ratios, reflecting the reduction in net displacement that occurs with increased deformation. Given that the surface of the Nullarbor Limestone retains a 15 million year record of upper crustal deformation, and the neotectonic stress regime is believed to have been initiated at approximately 8 Ma, reverse reactivation could conceivably explain the lower displacement values of the longer faults on the Eucla Platform. This scenario would imply that an extensional regime prevailed locally between 15 Ma and 8 Ma, before significant changes in plate boundary interactions sparked the onset of the neotectonic compressional regime.

6.3.2 Fault growth rates

It has been previously suggested that the Nullarbor Plain faults have not accumulated more than a few tens of metres of vertical slip over the last 15 million years, most commonly exhibiting less than 10 m of total vertical displacement (Clark et al., 2011). The displacement values obtained herein, which were derived in a more comprehensive manner that sought to neutralise the effects of karst topography, are partially in agreement. Whilst the maximum accumulated displacements generally didn't exceed 30 m (with the exception of faults nine and 19), all 27 faults actually exhibited peak displacements greater than 10 m. These revised peak displacement values correspond to slightly higher inferred fault growth rates across the platform.

In the case of fault nine, differential growth rates can be observed between the Nullarbor and Roe Plains expressions of the fault (2.0 m Ma^{-1} and 6.7 m Ma^{-1} respectively). This differential is also strikingly apparent in a comparison of growth rate statistics for faults manifested on each plain (Fig. 18). Assuming that the increased displacement rate on the younger Roe Plains (which is a calcarenite-veneered erosional surface cut ~80 m down into the platform) is not simply reflecting an increase in fault displacement at depth, this differential implies a strengthening of the neotectonic stress field since the Plio-Pleistocene.

6.3.3 Fault growth models

In the context of documented fault growth patterns around the globe, the Eucla Platform faults exhibit anomalously low 'displacement : scarp length' ratios. The traditional model of fault growth implies that faults accumulate displacement systematically with increases in scarp length (Cowie and Scholz, 1992; Walsh et al., 2002). Within this framework, established growth models would suggest that a 100 km long fault would exhibit a maximum displacement in the order of 1000 m (Fig. 19). The anomalously low displacement values recorded for the Eucla Platform faults may support an alternative model of fault growth described by Walsh et al. (2002), wherein scarp length is established early in the life of the fault and displacement accumulates thereafter (Fig. 19). Interestingly, this growth model is thought to be particularly applicable to reactivated fault systems (Walsh et al., 2002). Under this model, fault scarps developing over pre-existing structures increase in length until discrete fault segments begin to interact (i.e., fault linkage occurs). Such interaction can be recognised in the displacement profiles of certain fault sets across the platform, whereby a perturbation of the typical displacement pattern is evident in overlapping zones (Fig. 20). It should be noted that that the maximum vertical displacement values (and associated growth rates) presented herein have been calculated upon the premise that each of the selected faults is a discrete structure. If fault linkage patterns were to be assessed and accounted for, fault growth rate estimates would likely increase.

6.4 The Mundrabilla Fault and historic stress field partitioning

Given the scale and tectonic history of the Lasseter Shear Zone (the deep shear underlying the Mundrabilla Fault), the broader onshore influence of the Mundrabilla Fault on localised Cenozoic deformation should be re-assessed. The concept of the Lasseter Shear Zone (LSZ) was first proposed by Braun et al. (1991), as a mechanism by which enigmatic middle- to late-Palaeozoic stress field differentials could be explained. Stratigraphic evidence suggests that the centrally-located Eastern Officer, Amadeus, Ngalia and Wiso Basins underwent N-S compression from the Devonian to the Carboniferous, whilst the Canning and Bonaparte Basins (to the west) underwent contemporaneous N-S to NE-SW extension (Braun et al., 1991). This apparent partitioning of the palaeo-stress field between central and Western Australia was explained by the notion of the N-S trending LSZ, which is supported by a continent-scale gravity anomaly that divides the aforementioned basins (Fig. 3). The shear zone is thought to have accommodated sinistral movement in the Palaeozoic, although it has been acknowledged that a lack of evidence precludes a detailed assessment of its displacement history (Braun et al., 1991).

In the present-day Eucla Basin, the correlative Mundrabilla Fault seemingly coincides with a change in crustal thickness and geothermal gradient (Fig. 21). This supports the notion that the LSZ delineates a boundary in the underlying Proterozoic basement, potentially representing a focal point for the localised release of neotectonic strain (Clark et al., 2011). Given the central location of the Mundrabilla Fault on the Eucla Platform, its influence on Miocene to recent onshore deformation should be quantifiable through a comparison of fault characteristics either side of the structure. Additionally, any such influence should be manifested in the character of the modelled basal Nullarbor Limestone horizon. Figure 22 displays the fault scarp orientation data, partitioned to reflect the longitudinal position of the faults relative to the central Mundrabilla Fault. Whilst there are differences in the modal strike values either side of the Mundrabilla Fault, the total range of observed orientations do not vary significantly. Fault growth patterns are also indistinguishable either side of the Mundrabilla Fault (Fig. 23), as defined by an appropriately partitioned 'scarp length versus vertical displacement' graph. Furthermore, this consistency in the fault data is supported by the east-west continuity of the basal Nullarbor Limestone horizon, which doesn't exhibit any significant change in character across the Mundrabilla Fault (Fig. 12). Clearly, the major Palaeozoic stress field differentials associated with the Lasseter Shear Zone are not manifested on the present-day Eucla Platform via the Mundrabilla Fault.

7.0 Conclusions

A number of pertinent conclusions can be drawn from the data and analyses presented above. Whilst the investigation of subsurface horizons in the Cenozoic carbonate stratigraphy did not yield any significant evidence of intrabasinal folding or warping, it did highlight the effect that long-wavelength tilting has had on the basin's architecture. The degree of tilting measured on the basal Nullarbor Limestone horizon was shown to mirror that of the inboard Miocene palaeoshoreline, which supports the proposal that dynamic topography has been an important driver in the uplift of southwestern Australia over the last 15 million years.

With respect to the faults examined across the platform, the orientation of the prevailing stress field would imply that these structures share a neotectonic origin under a compressional regime. The inferred reverse dip-slip sense of displacement may well be complemented by an element of strike slip movement (i.e., oblique slip), as deduced from the anomalously low maximum vertical displacements exhibited along these faults. Analyses also revealed that reactivation has likely been an important process in the evolution of the

basin (as per the prevalence of deep magnetic signatures coinciding with many of the smaller faults), and regional fault development does not appear to have been influenced by the presence of the historically significant Mundrabilla Fault.

Cumulatively, the findings of this study carry broader implications. The lack of any significant intrabasinal warping of the sedimentary succession and the relatively subdued nature of documented fault movements clearly aligns with the notion of tectonic quiescence that has often been assigned to this region. Brittle deformation on the platform has not been an important landscape modifier at a basin-scale; rather, the extreme flatness of the platform disproportionately emphasises these features in the landscape. The study also highlights the apparent effectiveness of planation surfaces as tectonic benchmarks in a stable continental interior. This has important implications for ongoing sea level research, as the ability to detect warping on ancient surfaces will enable palaeoshoreline elevations to be further constrained.

8.0 Acknowledgements

I'd like to express my sincere appreciation to Dr Milo Barham and Dr Michael O'Leary for their constant guidance throughout the course of this project and the relentless enthusiasm they've shown towards my work. I am also very appreciative of the efforts of Dr Nick Timms, who provided ongoing counsel with respect to the structural geology components of the project. Thanks are extended to Assistant Professor Alan Aitken, Dr Mark Tingay, the Geological Survey of Western Australia (Dr Catherine Spaggiari) and the Geological Survey of South Australia for their valued assistance and input at various stages of the project.

9.0 References

Braun, J., McQueen, H., Etheridge, M., 1991. A fresh look at the late Palaeozoic tectonic history of western-central Australia. Exploration Geophysics 22, 49-54.

Burnett, S., Webb, J. A., and White, S., 2013. Shallow caves and blowholes on the Nullarbor Plain, Australia — Flank margin caves on a low gradient limestone platform. Geomorphology 201, 246-253.

Clark, D., McPherson, A., Collins, C., 2011. Australia's seismogenic neotectonic record : a case for heterogeneous intraplate deformation. Geoscience Australia, Canberra.

Clark, D., McPherson, A., Van Dissen, R., 2012. Long-term behaviour of Australian stable continental region (SCR) faults. Tectonophysics 566–567, 1-30.

Clarke, J.D.A., Gammon, P.R., Hou, B., Gallagher, S.J., 2003. Middle to Upper Eocene stratigraphic nomenclature and deposition in the Eucla Basin. Australian Journal of Earth Sciences 50, 231-248.

Cowie, P.A., Scholz, C.H., 1992. Displacement-length scaling relationship for faults: data synthesis and discussion. Journal of Structural Geology 14, 1149-1156.

Craig, R.S., 2002. The palaeobiogeography of Late Cretaceous and Cenozoic brachiopods from Western Australia. Palaeogeography, Palaeoclimatology, Palaeoecology 179, 267-292.

D'Ercole, C., Lockwood, A.M., 2003. The tectonic history of the Waigen area, western Officer Basin. Geological Survey of Western Australia, Perth, pp. 71-80.

Fossen, H., 2010. Structural Geology. Cambridge University Press, New York.

Heidbach, O., Tingay, M., Barth, A., Reinecker, J., Kurfeb, D., Muller, B., 2008. The World Stress Map Database. http://dc-app3-14.gfz-potsdam.de/pub/casmo/casmo_frame.html (accessed 15 September 2013).

Hillis, R.R., Sandiford, M., Reynolds, S.D., Quigley, M.C., 2008. Present-day stresses, seismicity and Neogene-to-Recent tectonics of Australia's 'passive' margins: intraplate deformation controlled by plate boundary forces. Geological Society of London Special Publication 306, 71-90.

Holgate, F.L., Gerner, E.J., 2008. OZTemp Well Temperature Data. http://www.ga.gov.au/meta/ANZCW0703013802.html (accessed 10 September 2013).

Hou, B., Frakes, L.A., Sandiford, M., Worrall, L., Keeling, J., Alley, N.F., 2008. Cenozoic Eucla Basin and associated palaeovalleys, southern Australia — Climatic and tectonic influences on landscape evolution, sedimentation and heavy mineral accumulation. Sedimentary Geology 203, 112-130.

James, N.P., Bone, Y., 1991. Origin of a cool-water, Oligo-Miocene deep shelf limestone, Eucla Platform, southern Australia. Sedimentology 38, 323-341.

James, N.P., Bone, Y., 2000. Eocene cool-water carbonate and biosiliceous sedimentation dynamics, St Vincent Basin, South Australia. Sedimentology 47, 761-786.

James, N.P., Bone, Y., 2007. A late Pliocene–early Pleistocene, inner-shelf, subtropical, seagrass-dominated carbonate: Roe Calcarenite, Great Australian Bight, Western Australia. Palaios 22, 343-359.

James, N.P., Bone, Y., Carter, R.M., Murray-Wallace, C.V., 2006. Origin of the Late Neogene Roe Plains and their calcarenite veneer: Implications for sedimentology and tectonics in the Great Australian Bight. Australian Journal of Earth Sciences 53, 407-419.

Johnson, D., 2004. The Geology of Australia. Cambridge University Press, Cambridge.

Kim, Y.-S., Sanderson, D.J., 2005. The relationship between displacement and length of faults: a review. Earth-Science Reviews 68, 317-334.

Laske, G., Masters, G., Reif, C., 2013. Crust 2.0: A New Global Crustal Model at 2x2 Degrees. http://igppweb.ucsd.edu/~gabi/crust2.html (accessed 10 September 2013).

Li, Q., James, N.P., Bone, Y., McGowran, B., 1996. Foraminiferal biostratigraphy and depositional environments of the mid-Cenozoic Abrakurrie Limestone, Eucla Basin, southern Australia. Australian Journal of Earth Sciences 43, 437-450.

Li, Q., James, N.P., McGowran, B., 2003. Middle and Late Eocene Great Australian Bight lithobiostratigraphy and stepwise evolution of the southern Australian continental margin. Australian Journal of Earth Sciences 50, 113-128.

Lowry, D.C., 1967. Tertiary stratigraphic units in the Eucla Basin in Western Australia. Geological Survey of Western Australia (Article), Perth.

Lowry, D.C., 1970. Geology of the Western Australian part of the Eucla Basin. Geological Survey of Western Australia (Bulletin 122), Perth.

McGowran, B., 1972. Rifting and drift of Australia and the migration of mammals. Science 180, 759-761.

McGowran, B., Li, Q., Cann, J., Padley, D., McKirdy, D.M., Shafik, S., 1997. Biogeographic impact of the Leeuwin Current in southern Australia since the late middle Eocene. Palaeogeography, Palaeoclimatology, Palaeoecology 136, 19-40.

O'Connell, L.G., 2011. Sedimentology of the Miocene Nullarbor Limestone, southern Australia. Geological Survey of Western Australia (Report 111), Perth.

O'Connell, L.G., James, N.P., Bone, Y., 2012. The Miocene Nullarbor Limestone, southern Australia; deposition on a vast subtropical epeiric platform. Sedimentary Geology 253-254, 1-16.

Quigley, M.C., Clark, D., Sandiford, M., 2010. Tectonic geomorphology of Australia. Geological Society of London Special Publication 'Australian landscapes' 346, 243-265.

Sandiford, M., 2007. The tilting continent: A new constraint on the dynamic topographic field from Australia. Earth and Planetary Science Letters 261, 152-163.

Stagg, H.M.J., Willcox, J.B., Symonds, P.A., O'Brien, G.W., Colwell, J.B., Hill, P.J., Lee, C.S., Moore, A.M.G., Struckmeyer, H.I.M., 1999. Architecture and evolution of the Australian continental margin. AGSO Journal of Australian Geology and Geophysics 17, 17-33.

Veevers, J.J., 1984. Phanerozoic Earth History of Australia. Clarendon Press, Oxford.

Veevers, J.J., 2000. Change of tectono-stratigraphic regime in the Australian plate during the 99 Ma (mid-Cretaceous) and 43 Ma (mid-Eocene) swerves of the Pacific. Geology 28, 47-50.

Walsh, J.J., Nicol, A., Childs, C., 2002. An alternative model for the growth of faults. Journal of Structural Geology 24, 1669-1675.

Walsh, J.J., Watterson, J., 1988. Analysis of the relationship between displacements and dimensions of faults. Journal of Structural Geology 10, 239-247.

Webb, J.A., James, J.M., 2006. Karst evolution of the Nullarbor Plain, Australia. Geological Society of America (special paper) 404, 65-78.

10.0 Figures

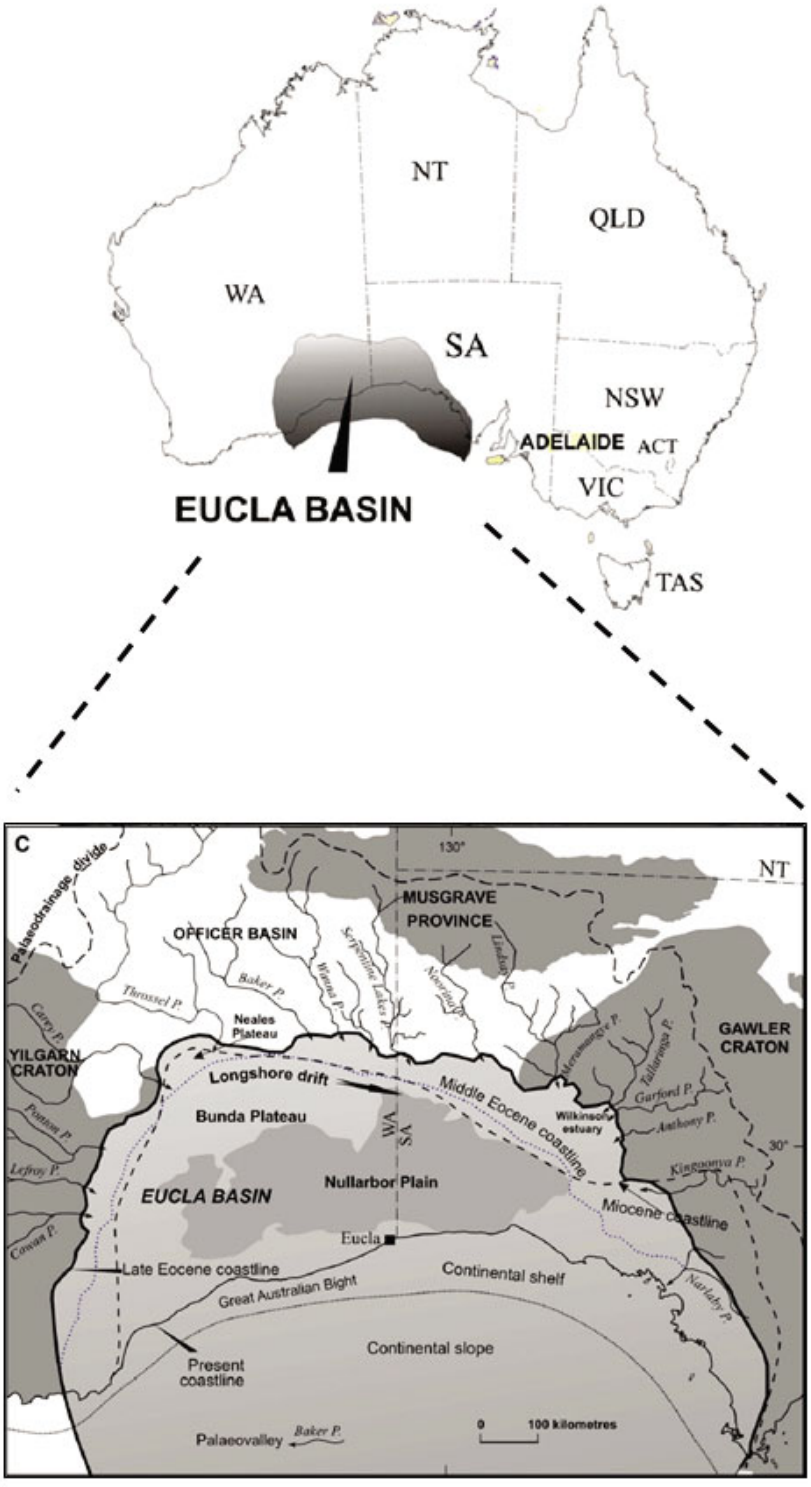

Figure 1: A map depicting the location and extent (both onshore and offshore) of the Eucla Basin. Taken from Hou et al. (2008).

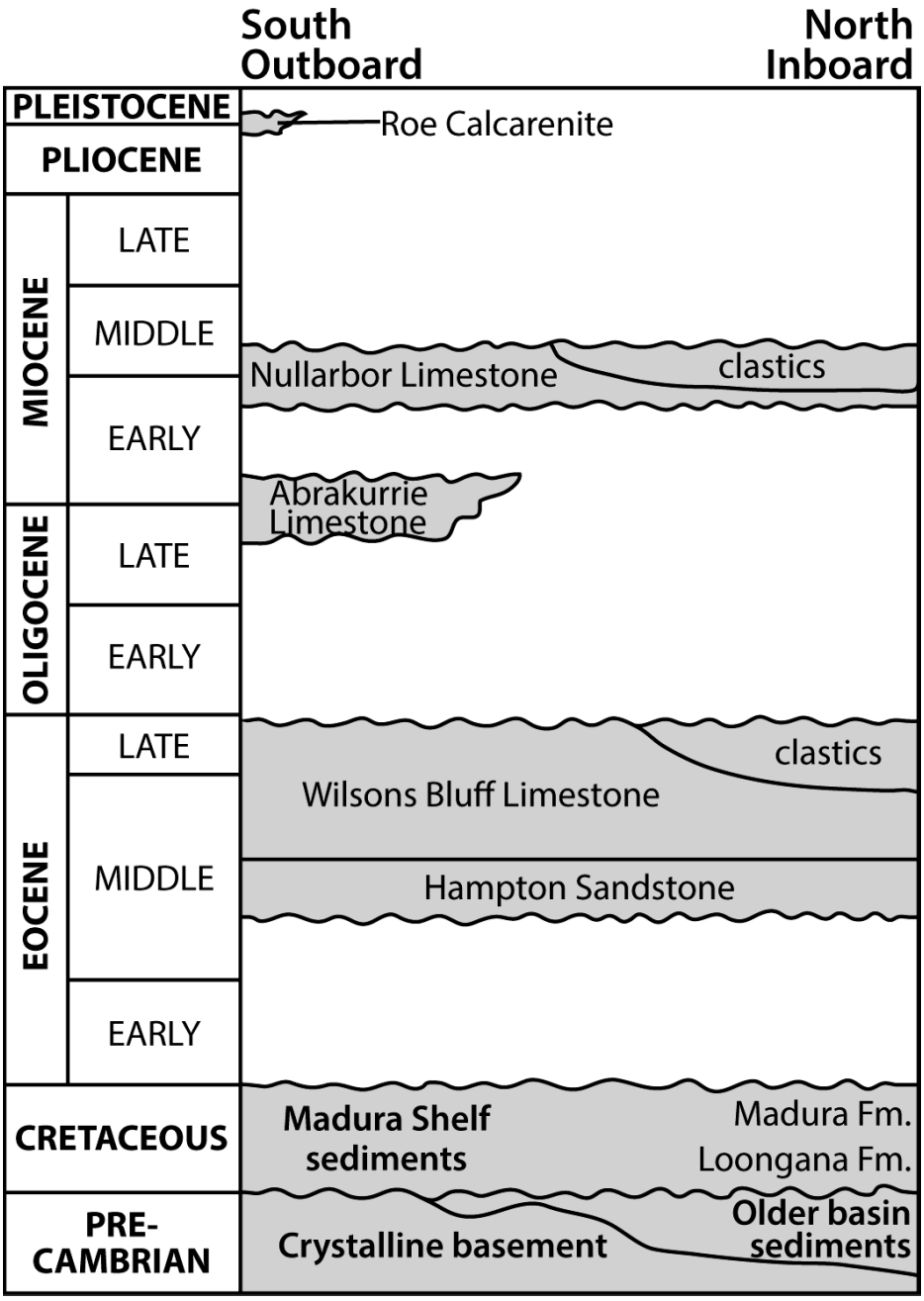

Figure 2: Stratigraphic chart of the Cenozoic Eucla Basin, highlighting the relative age and stratigraphic position of the 'Eucla Group' (Eocene to Miocene carbonate units) sedimentary succession. Modified from O'Connell et al., (2012).

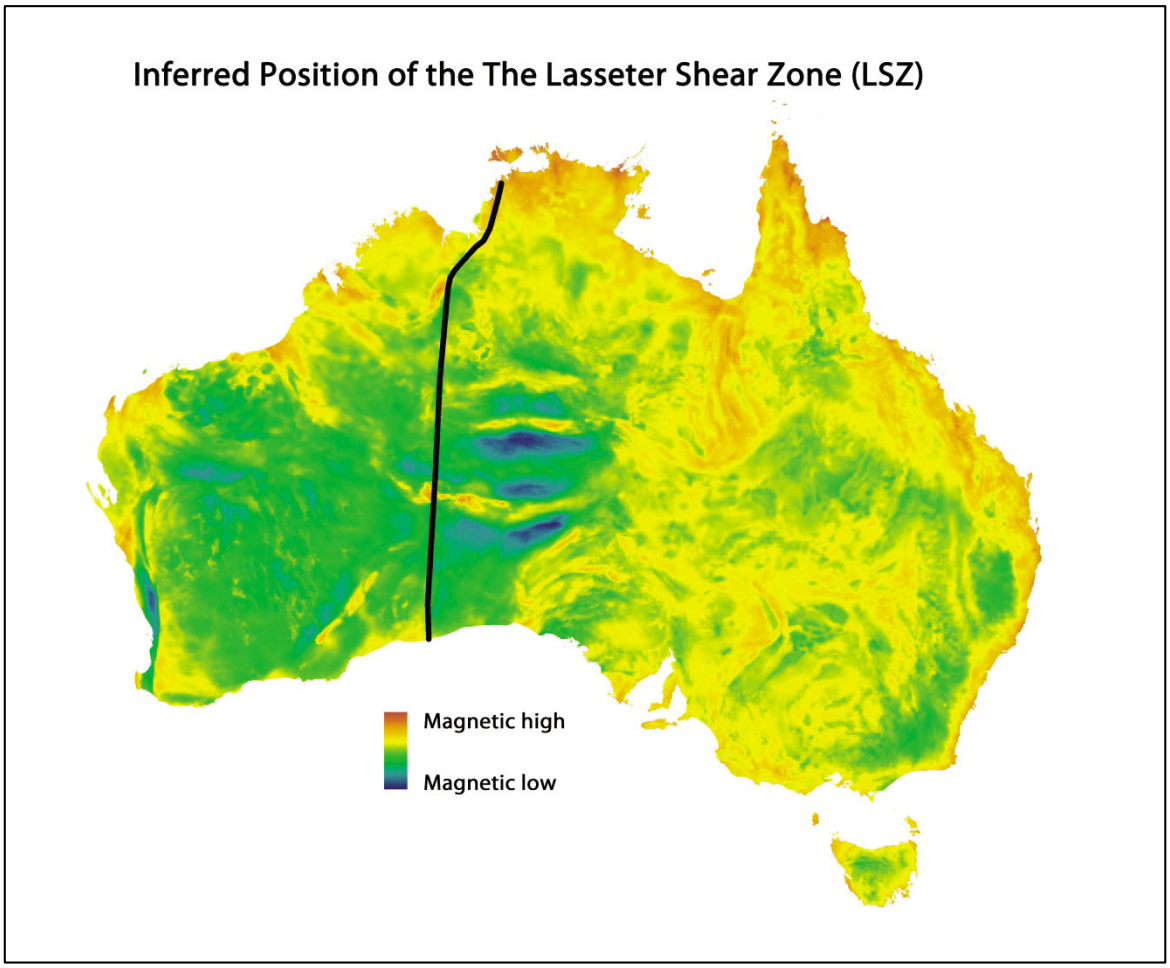

Figure 3: The position of the continent-scale Lasseter Shear Zone (LSZ), as inferred by Braun et al. (1991). The Mundrabilla Fault directly overlies this shear on the Nullarbor Plain. Figure adapted from Braun et al. (1991); gravity data sourced from Geoscience Australia.

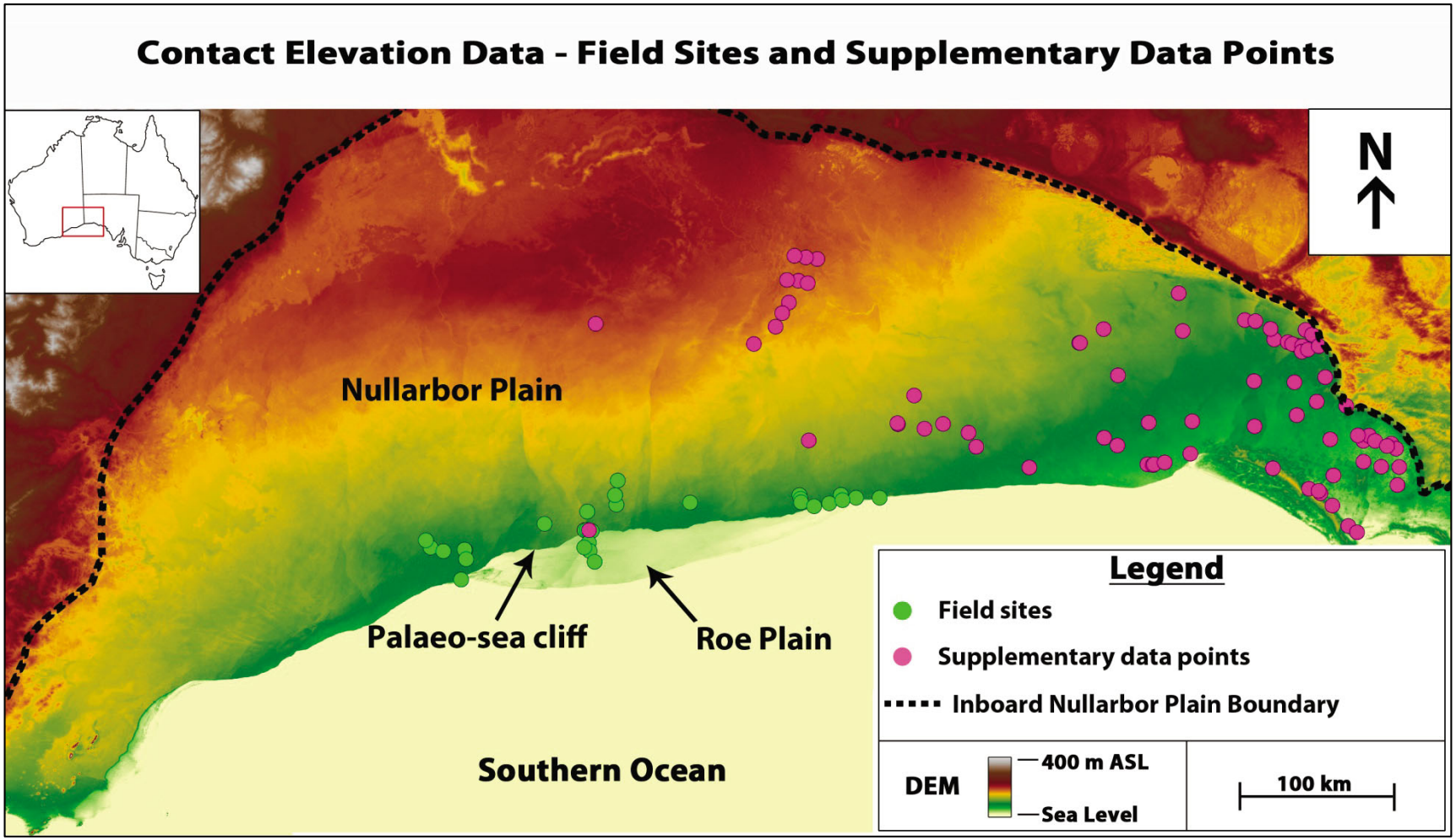

Figure 4: The locations of the 27 field sites and the 75 additional sites (from which supplementary elevation data was obtained), overlain on a digital elevation model.

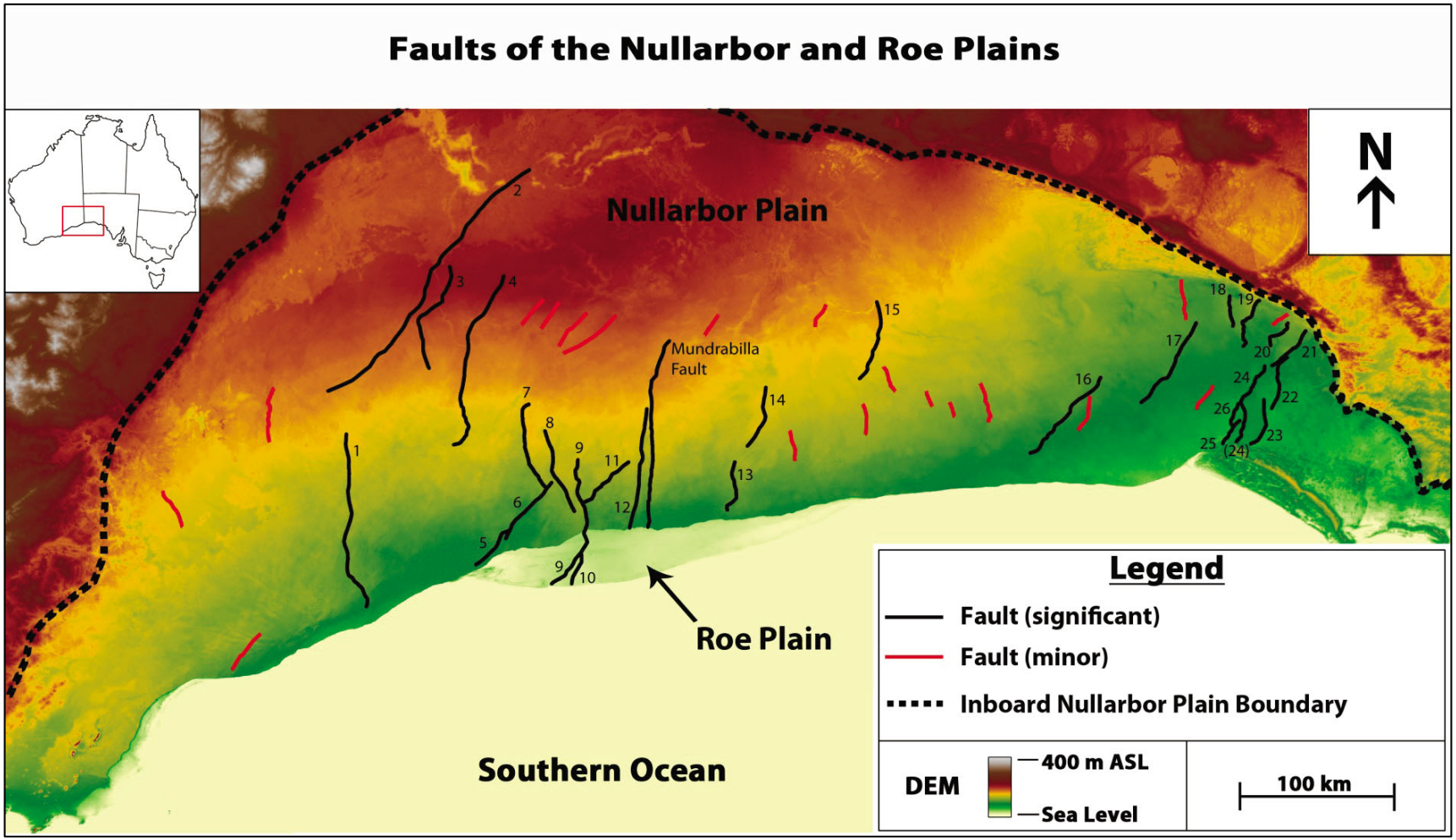

Figure 5: Fault traces for the 46 Nullarbor and Roe Plains faults considered in the analysis. Those depicted in black were deemed significant (with respect to scarp length and/or vertical displacement), whilst those depicted in red were deemed minor. Vertical displacement profiles were generated for significant faults only, whilst all faults were incorporated into the fault trend analysis.

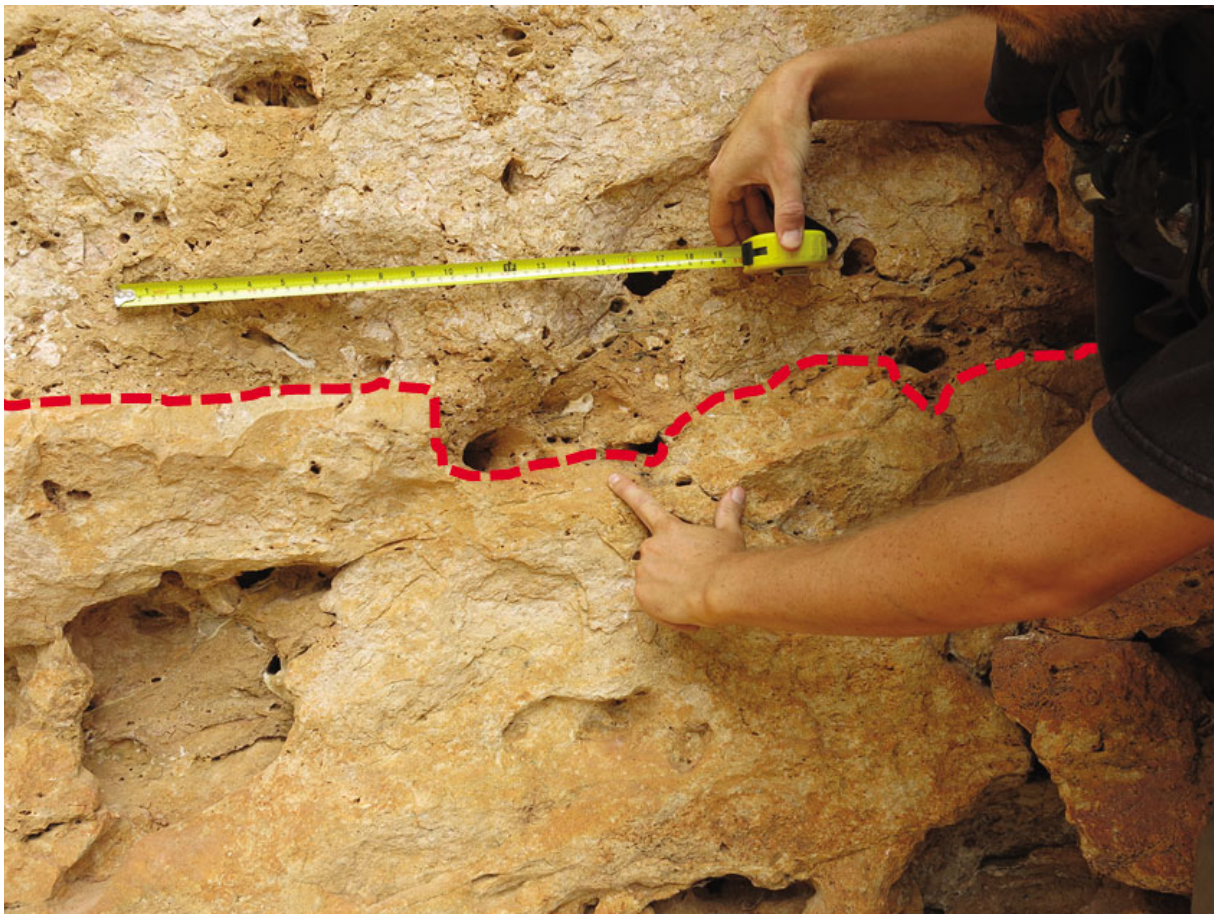

Figure 6: The expression of the contact between the Abrakurrie Limestone (bottom) and the Mullamullang Member of the Nullarbor Limestone (top) at Kutawala Cave. Localised karstic dissolution generated approximately 10 cm of relief along an otherwise relatively planar contact (50 cm tape measure for scale). This was one of the most pronounced examples of karst alteration noted along any fossil planation surface in the field (photo L. Mounsher).

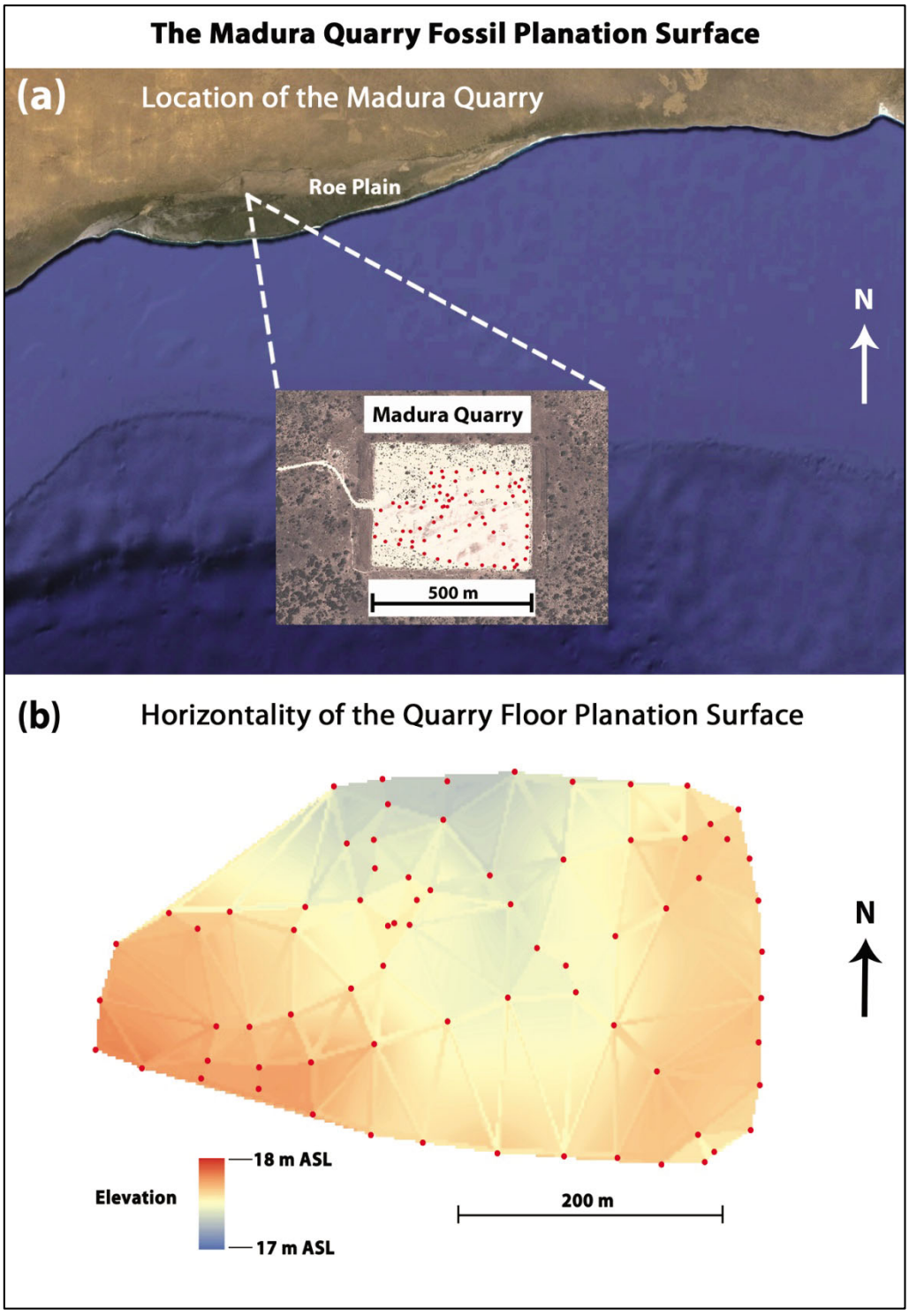

Figure 7: The location of the Madura Quarry (a), wherein 75 elevation data points were acquired for the basal Roe Calcarenite planation surface (data points are shown in red). Modelling of the 2 Ma planation surface over an area of approximately 130,000 m^2 revealed a striking degree of horizontality (b).

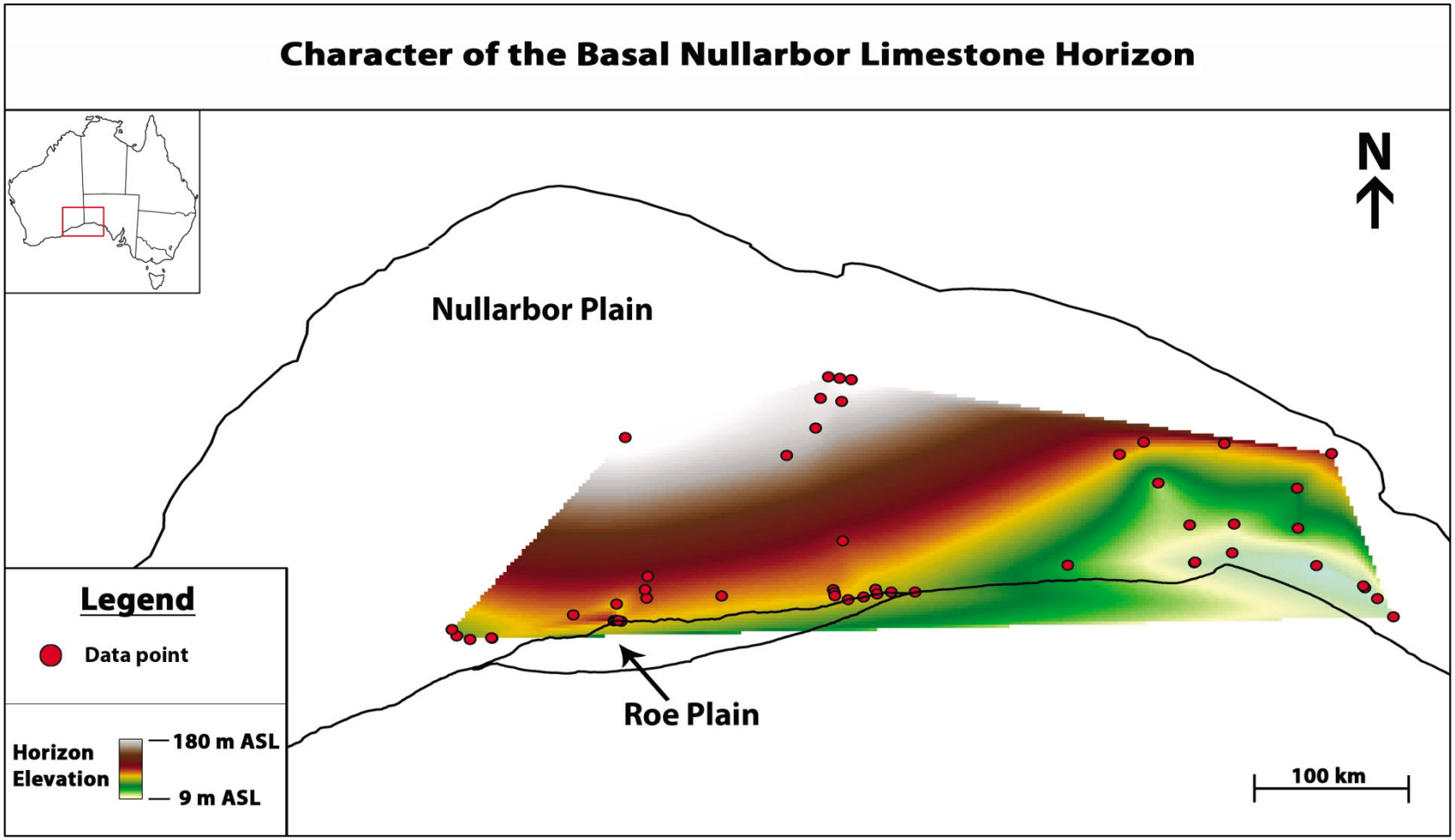

Figure 8: A model depicting the character of the basal Nullarbor Limestone horizon. Red data points represent sites at which the elevation of this particular horizon was attainable (both field sites and supplementary data sites). The horizon appears to be tilting about a NE-SW axis.

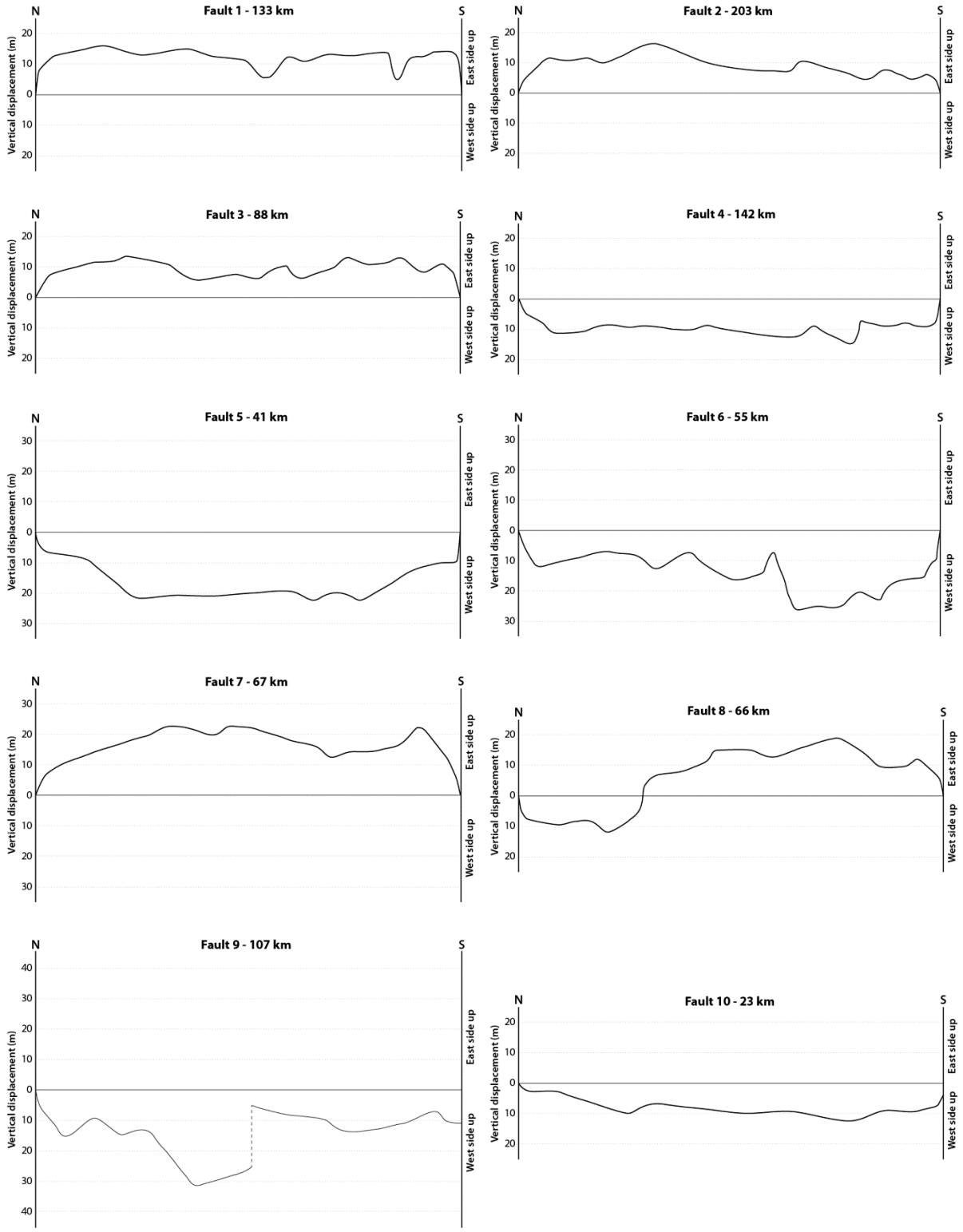

Figure 9 (part 1/3): Vertical displacement profiles for the 27 faults deemed to be significant (see Figure 5 for fault locations). Note that profiles representing faults that are situated on the perimeter of the Nullarbor or Roe Plains (i.e. faults 9, 10, 19, 21, 23, 24 and 25) do not depict complete fault closure at one end of the fault. This reflects the continuation of the structure beyond the study area.

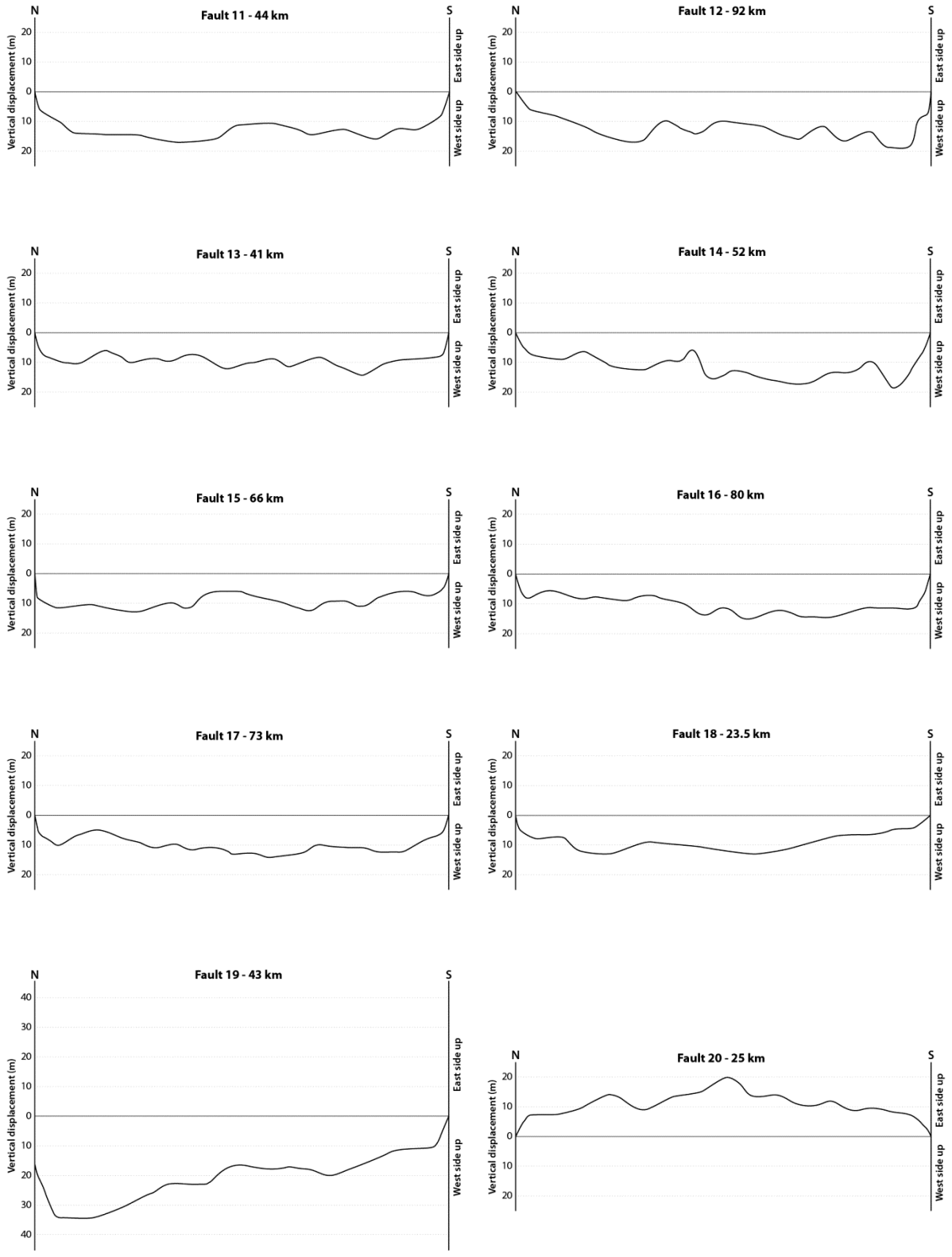

Figure 9 continued (part 2/3)

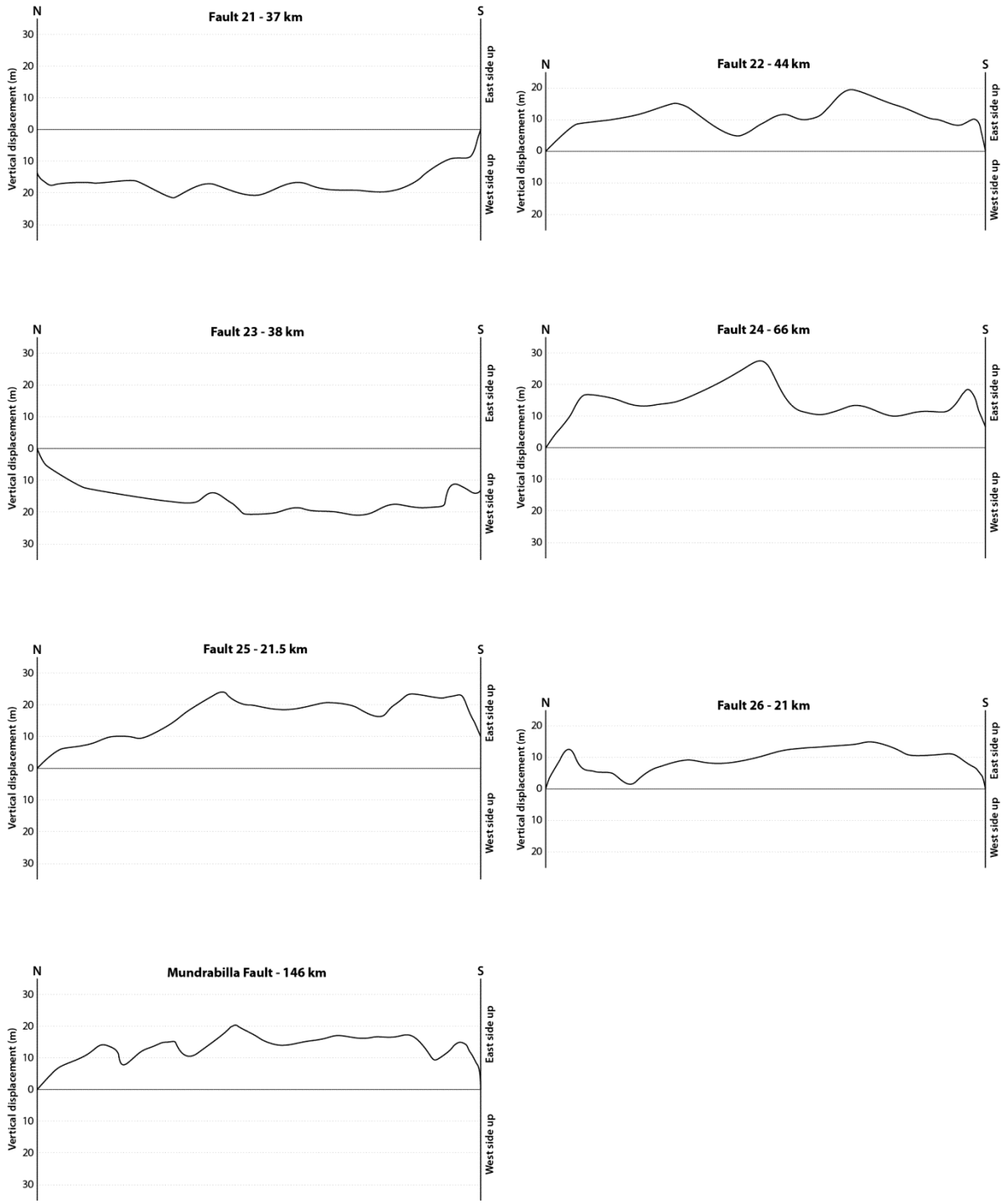

Figure 9 continued (part 3/3)

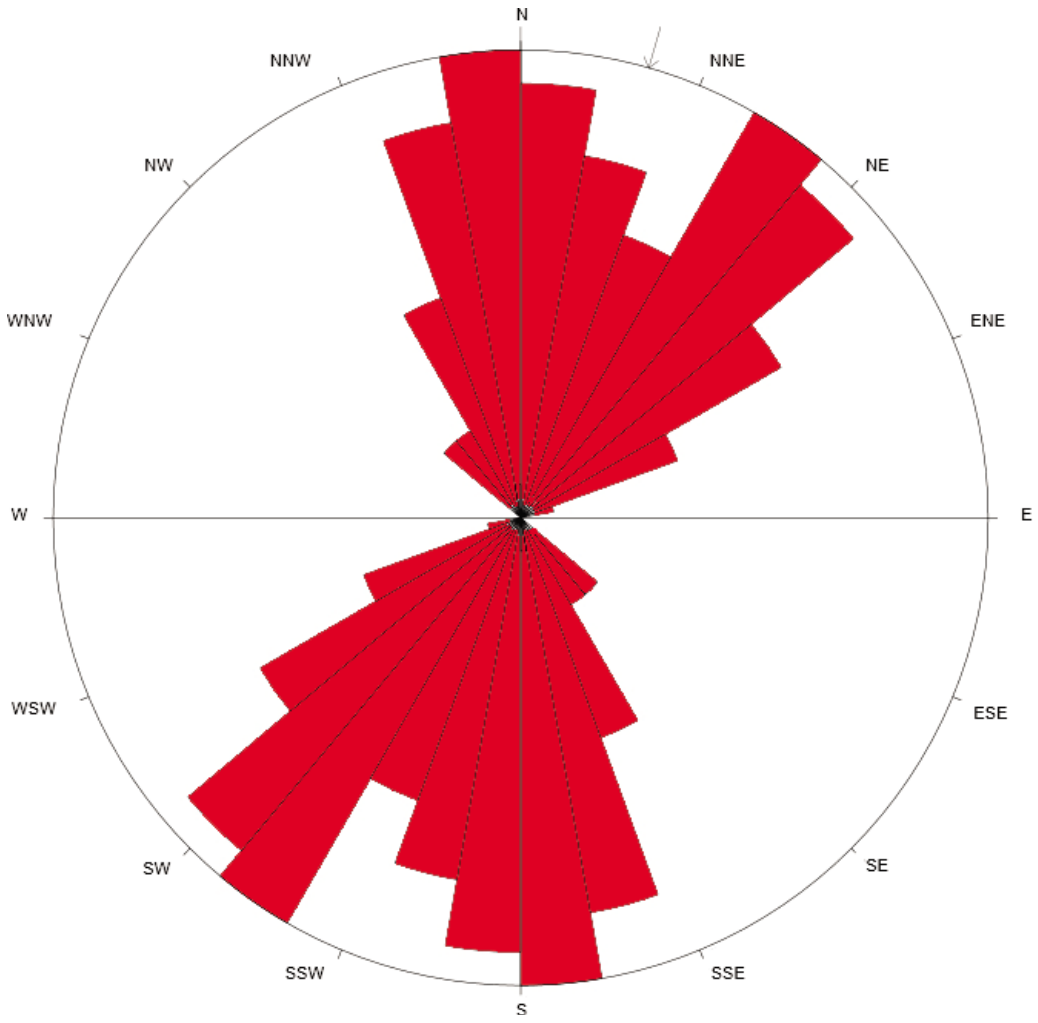

Figure 10: A rose diagram depicting the strike orientation of faults (and discretely-oriented fault segments) across the Nullarbor and Roe Plains. The mean strike value (016) is denoted by an arrow. Bin intervals are 10° and the highest data frequency in any one interval is 14. The total data set represents 115 strike measurements.

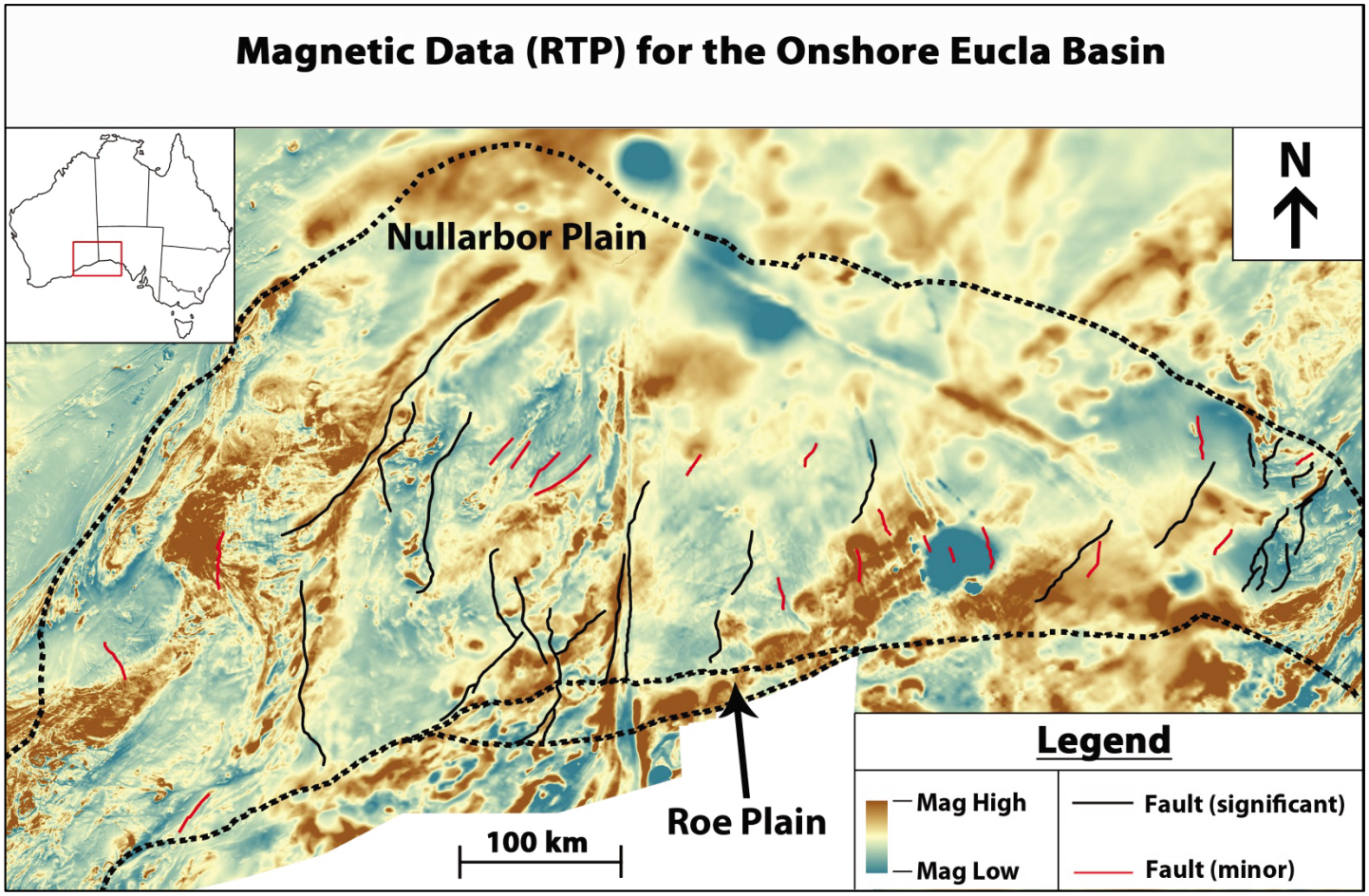

Figure 11: Magnetic data (reduced to pole) acquired over the onshore portion of the Eucla Basin. The majority of the faults deemed significant (marked in black), and many of the minor faults (red) are clearly represented in the geophysical data. In certain instances (e.g. fault two, 12, 15 and the Mundrabilla Fault; see figure 5 for fault numbering), the corresponding magnetic anomalies can be seen to extend well beyond the surface faults themselves. Aeromagnetic data retrieved from Geoscience Australia.

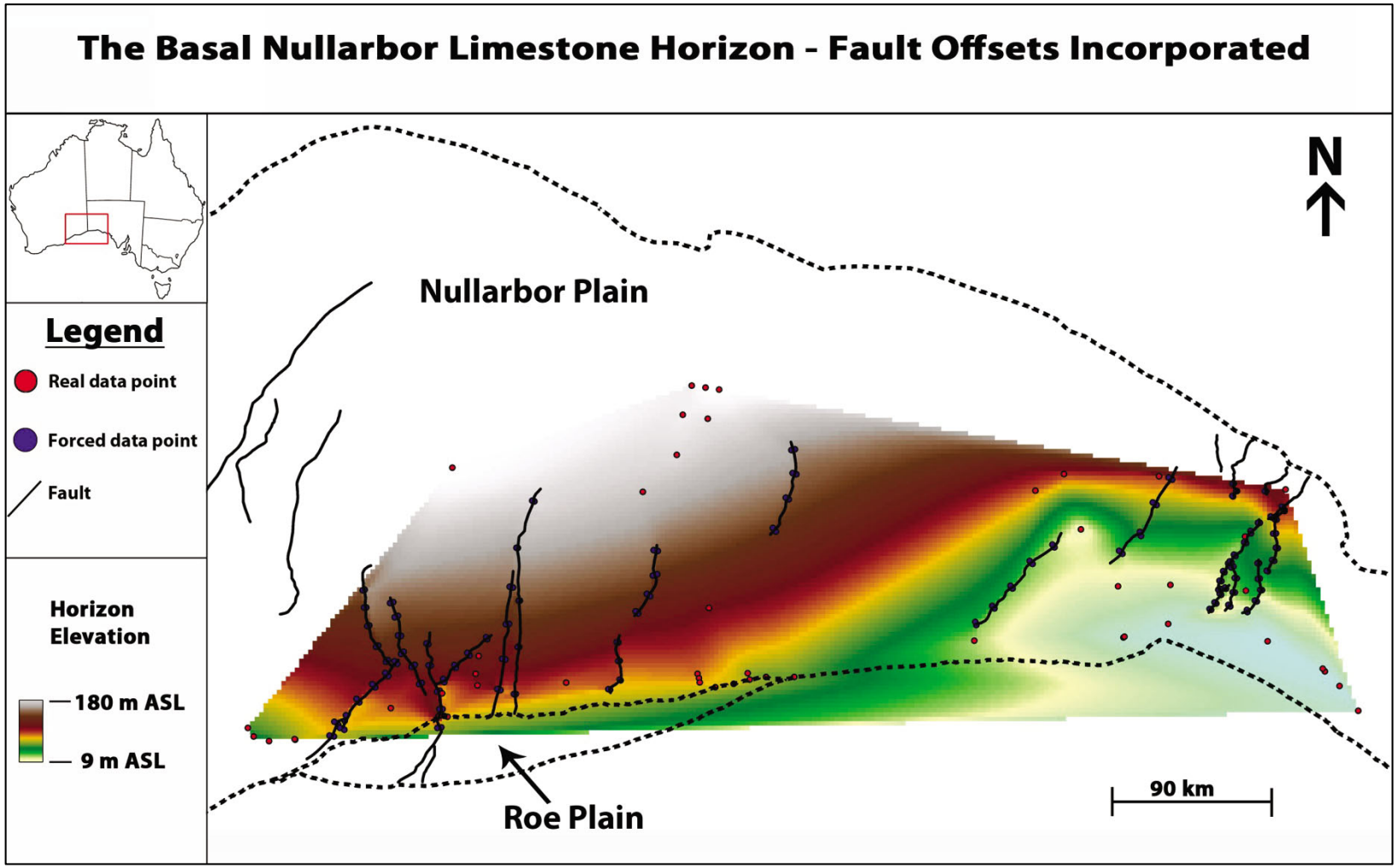

Figure 12: The incorporation of fault displacement data into the basal Nullarbor Limestone horizon highlights the negligible influence of faulting on the basin-scale character of sediments. Red dots represent real horizon elevation data points, whilst blue dots represent pairs of fault offset data points (straddling each fault) that were 'forced' into the model.

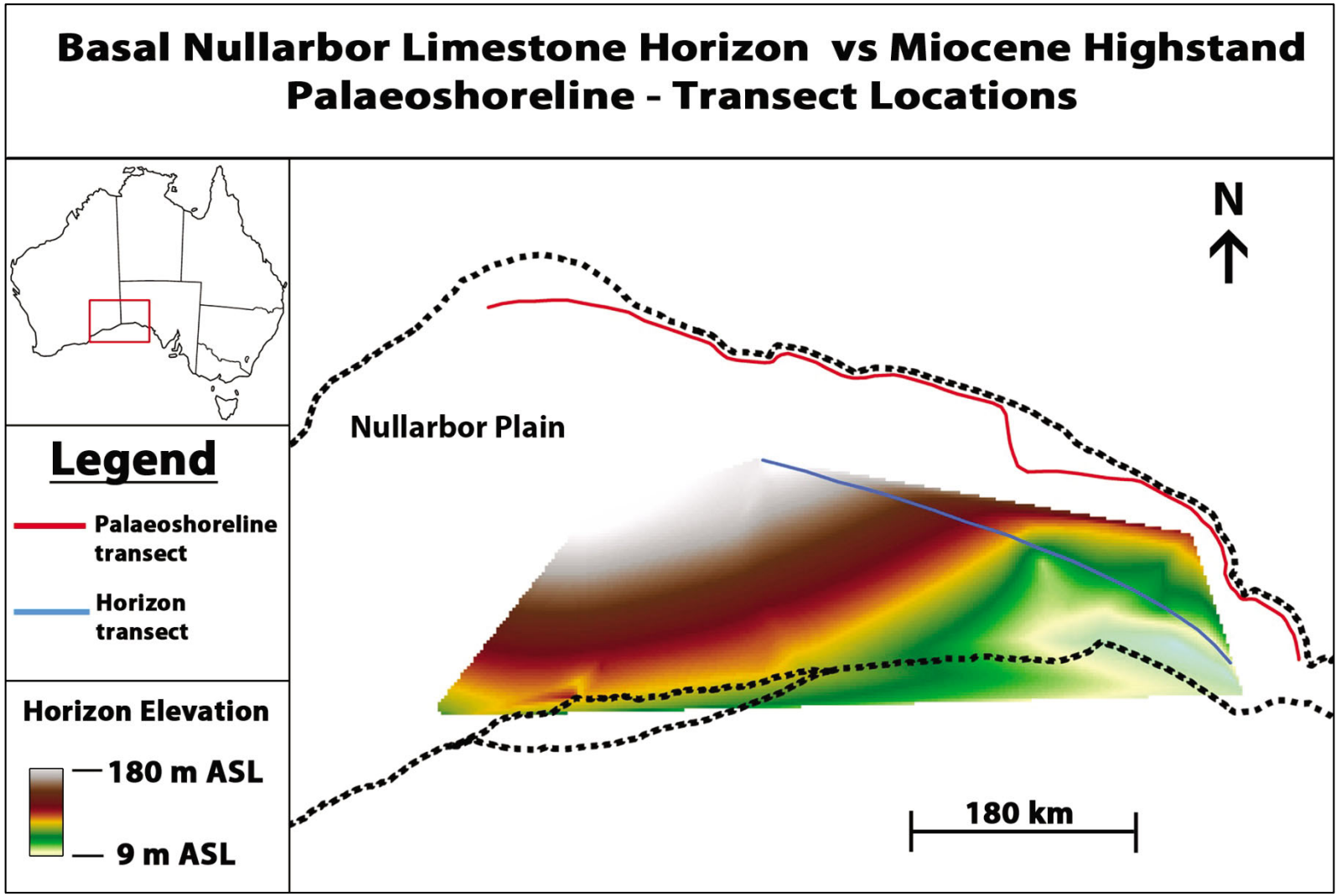

Figure 13: Locations of the approximately E-W transects across the Miocene palaeoshoreline (red; Sandiford, 2007) and the basal Nullarbor Limestone horizon (blue; this work).

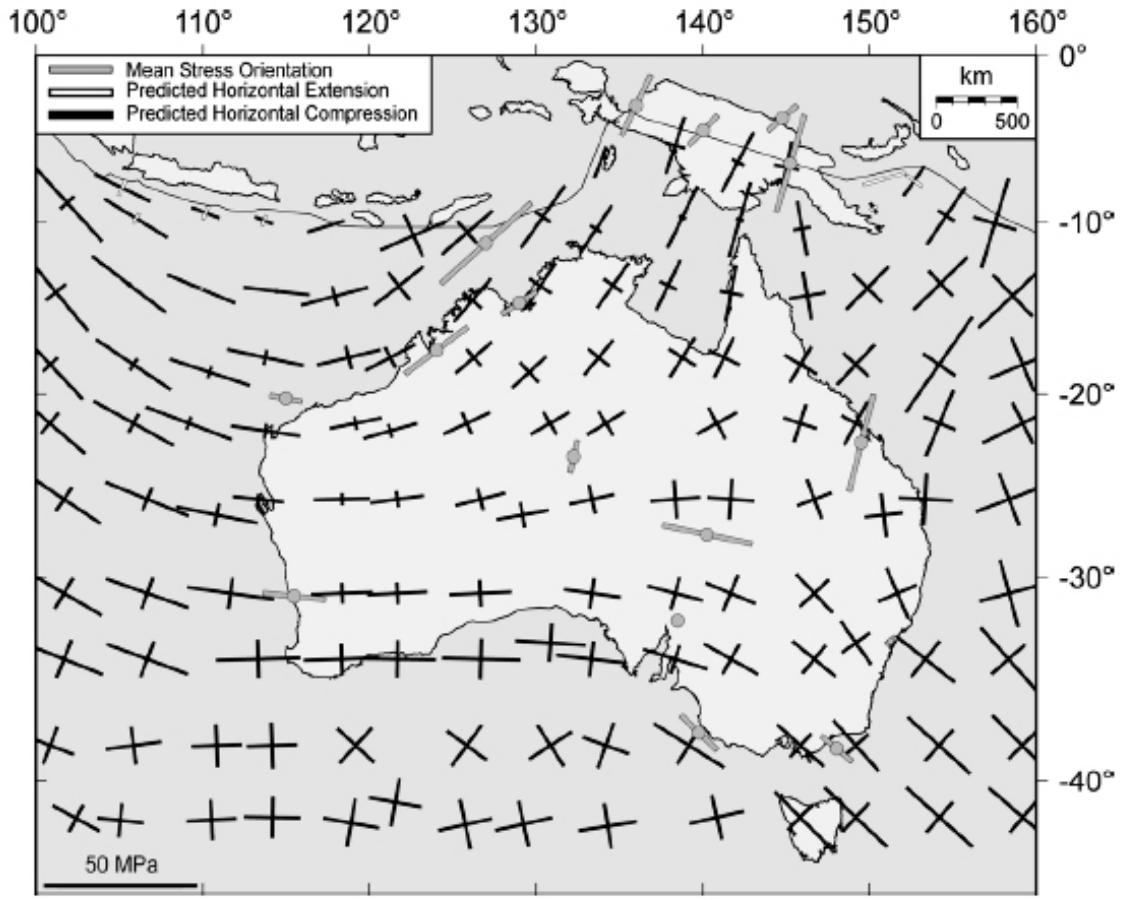

Figure 14: The continent-scale neotectonic stress field, as predicted from plate boundary force modelling, infers an E-W oriented maximum horizontal stress (σ_{Hmax}) for the onshore Eucla Basin region. Figure from Hillis et al. (2008).

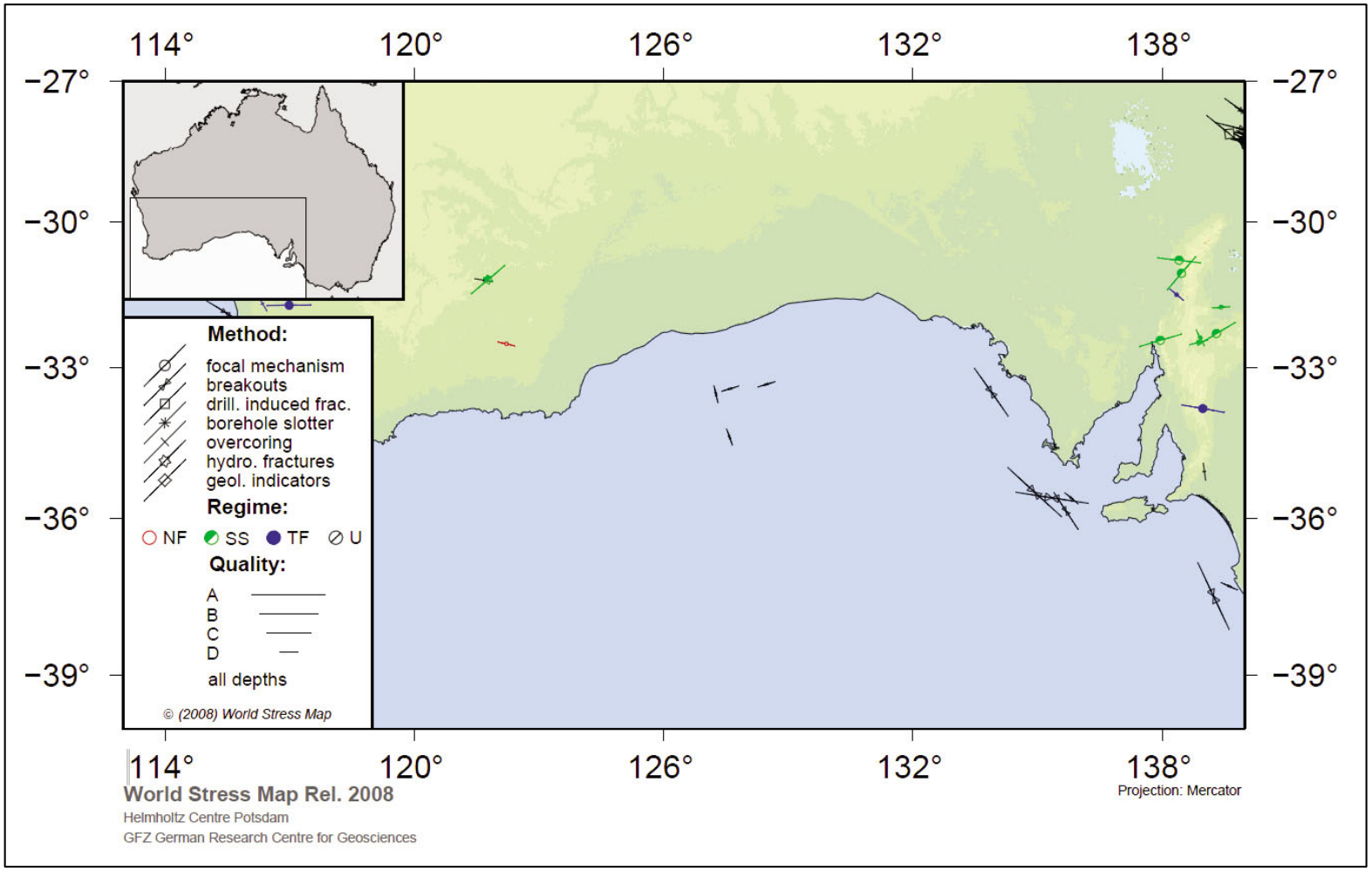

Figure 15: Map of the southern margin displaying the limited stress data available for the Eucla Basin surrounds. Stress indicators represent the σ_{Hmax} direction; colours correspond to different regimes. The data quality rating (A-D) assigned to each site reflects the number, accuracy and depth of stress field measurements. Figure from Heidbach et al. (2008).

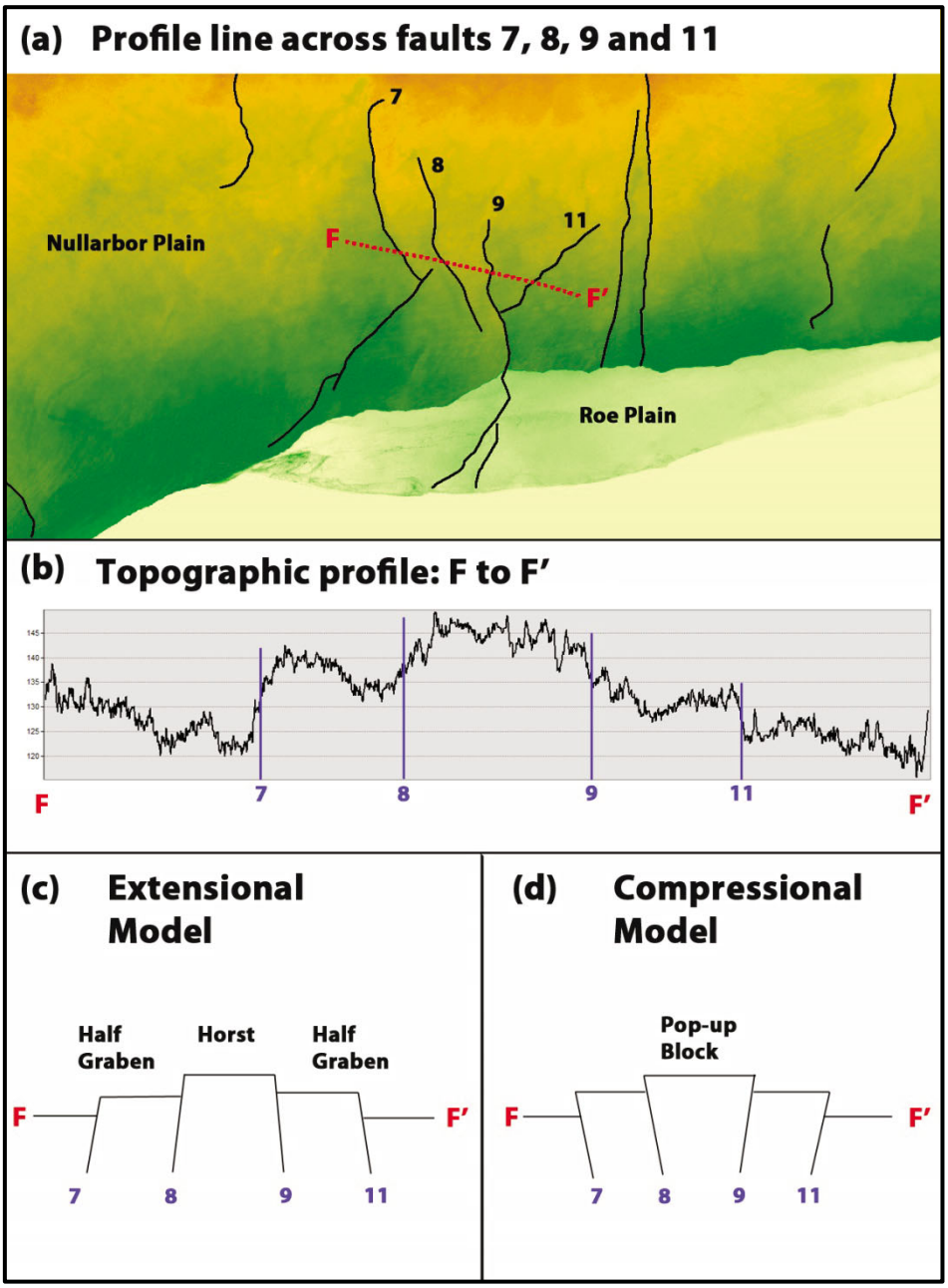

Figure 16: An example of the ambiguity encountered when examining fault system kinematics on the karstified Eucla Platform. A transect drawn across the fault system defined by faults 7, 8, 9 and 11 (a) produces the above topographic profile (b). Note that the fault plane locations in (b) are denoted by vertical blue lines. The surficial expression of this system could plausibly have been generated under either an extensional regime (c) or a compressional regime (d).

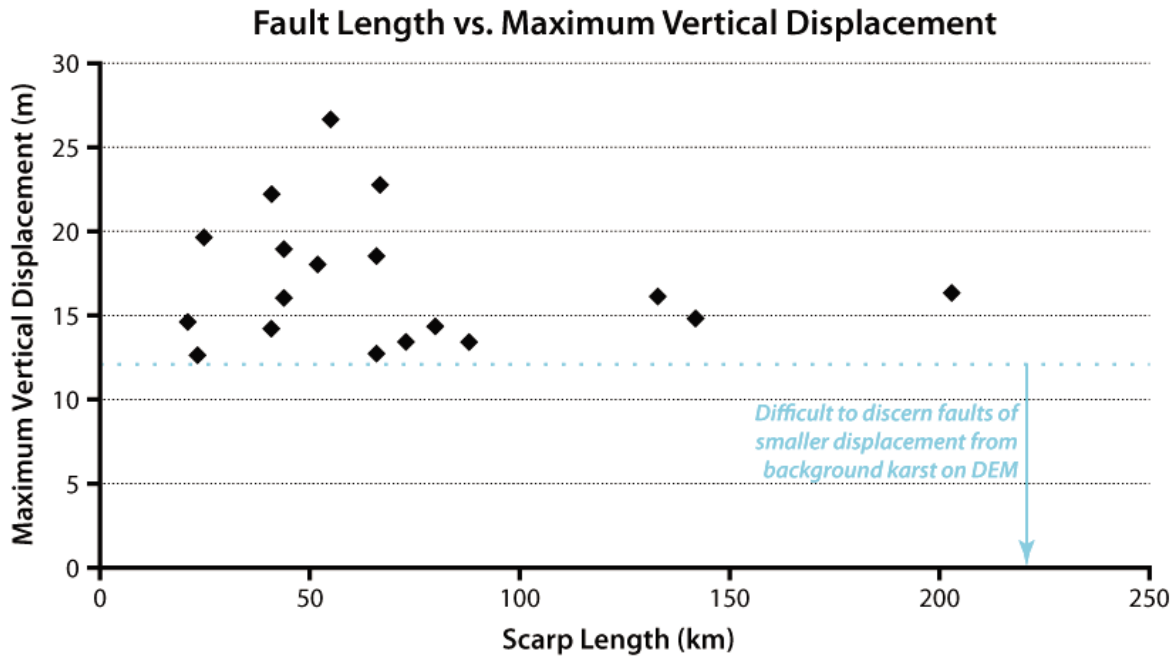

Figure 17: Characterisation of the onshore faults according to their respective 'scarp length to displacement' ratios. Given that fault displacements have been measured in the vertical plane, dip slip faults would be expected to display a characteristic increase in displacement with scarp length. This pattern is not evident in the Eucla Platform faults (especially those with longer fault scarps), and accordingly, strike slip movement could be inferred.

Note: all faults that have been shown to continue beyond the study area (i.e. those for which finite maximum displacement values and scarp lengths are not known) have been eliminated from this analysis.

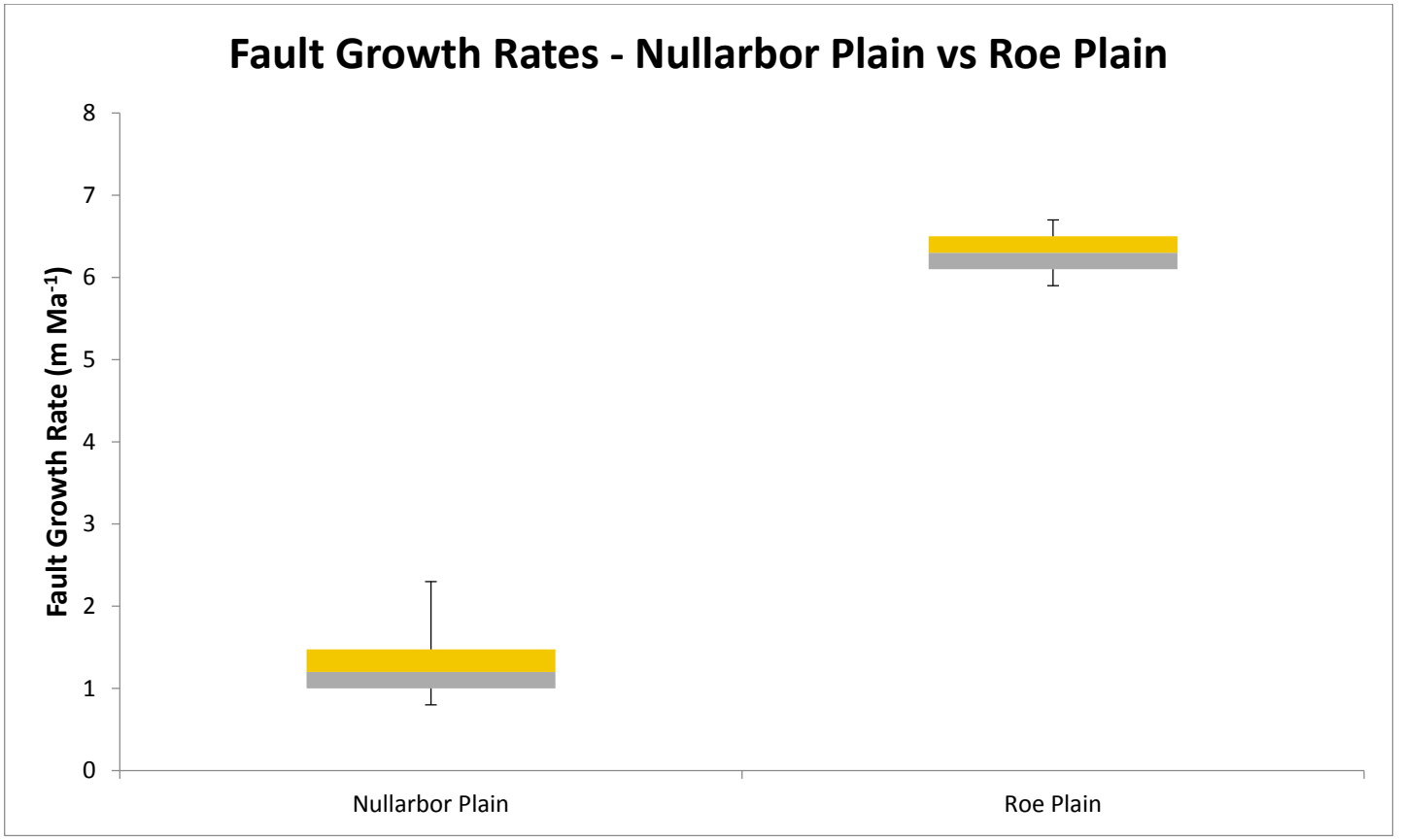

Figure 18: A comparison of growth rates (m Ma^{-1}) for faults occurring on the Nullarbor and Roe Plains. The box plots depict the minimum, 25th percentile, 50th percentile (median), 75th percentile and maximum growth rates. Note that the statistical significance of the comparison is limited by the small number of faults manifested on the Roe Plains (n=2).

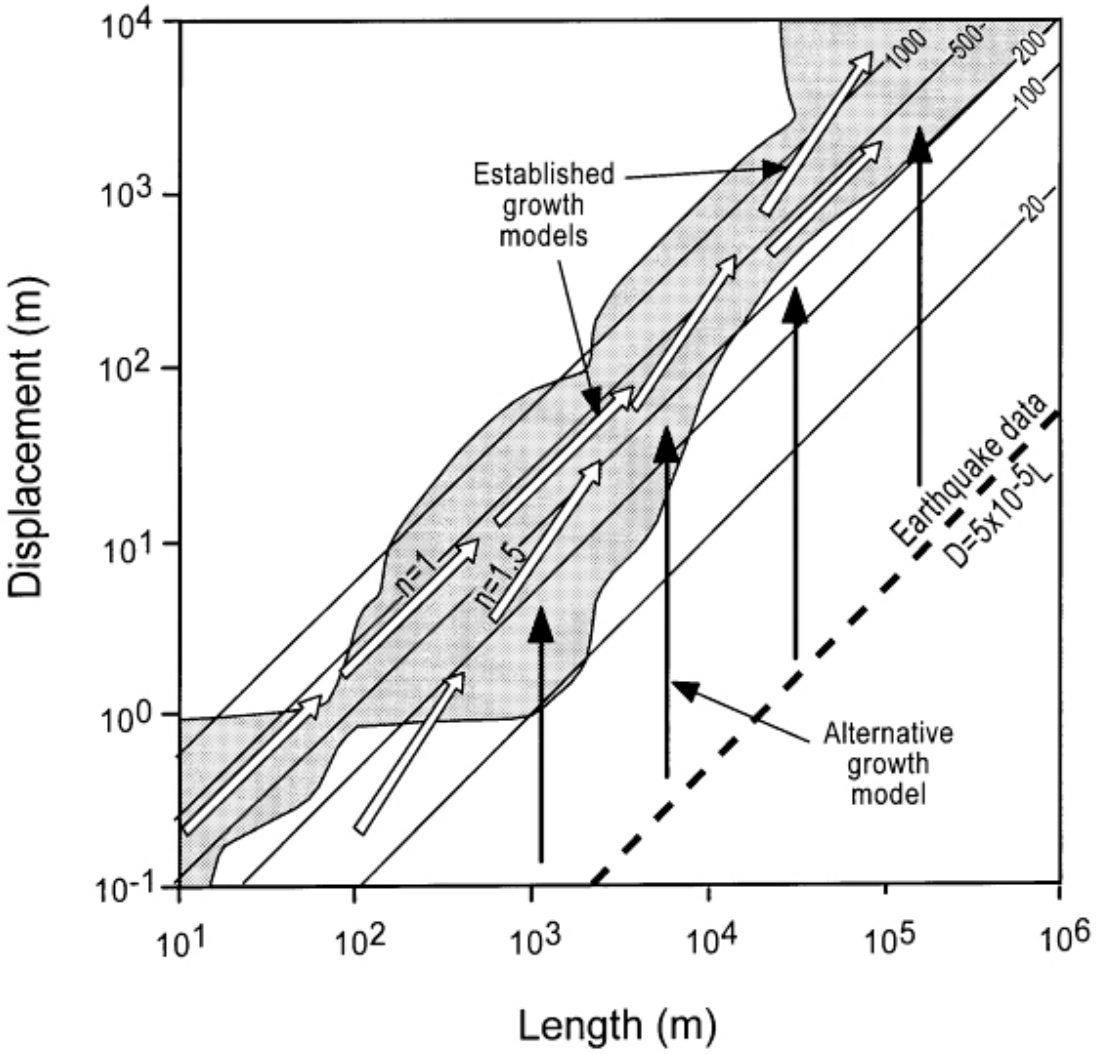

Figure 19: Established fault growth models, depicted by the white arrows, predict that faults grow by a systematic increase in fault scarp length and displacement through time. The alternative model proposed by Walsh et al. (2002) suggests that scarp lengths are established very early in the growth history of the fault, and displacement accumulates thereafter (this pattern is depicted by black arrows). Image taken from Walsh et al. (2002).

(a)

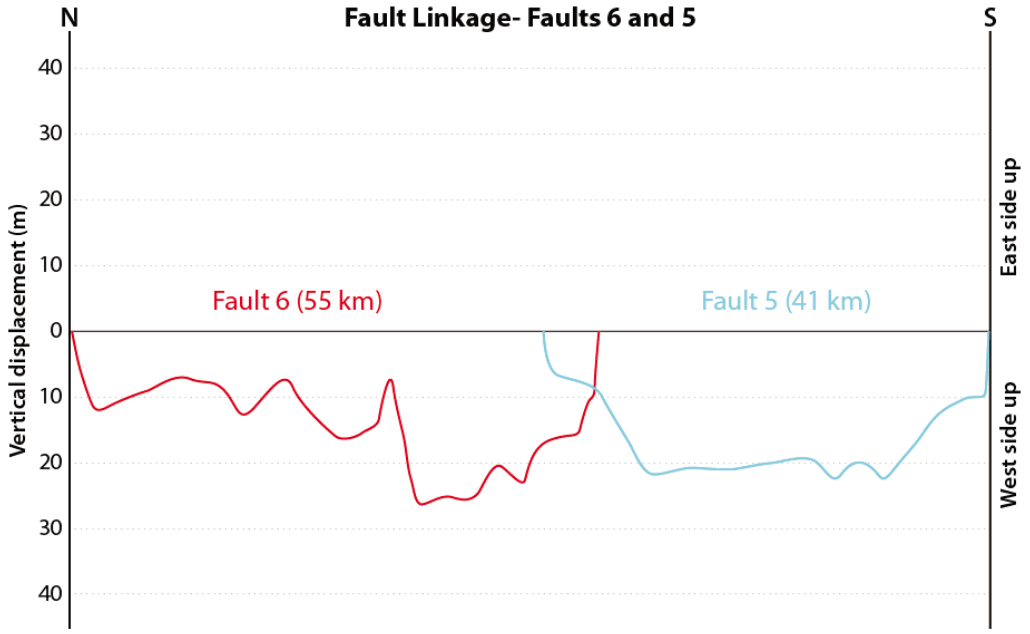

(b)

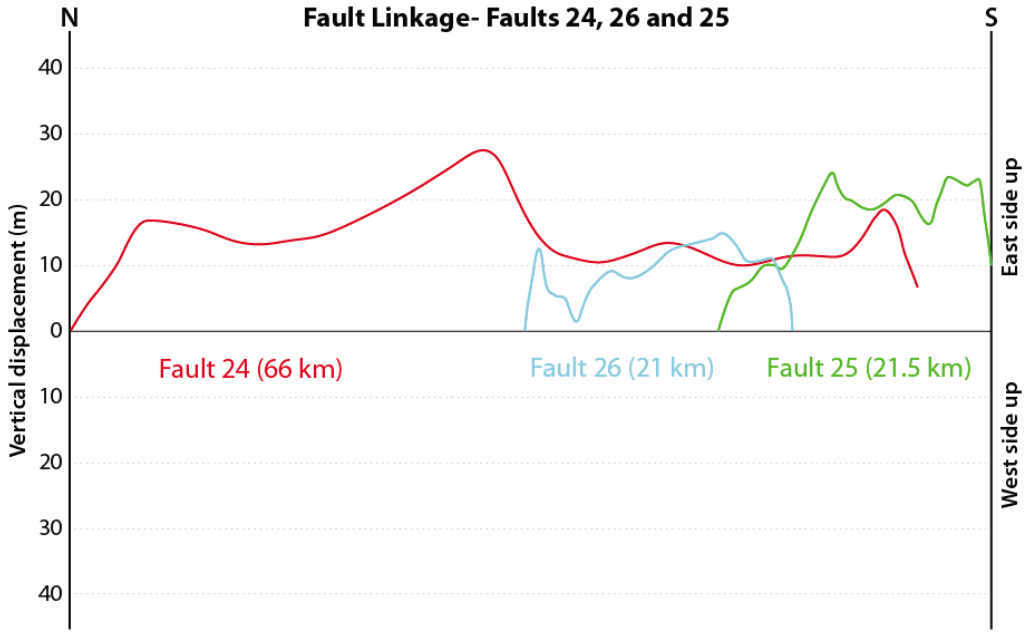

Figure 20: Evidence of fault linkage on the Eucla Platform. In cases (a) and (b), perturbation of the respective displacement profiles can be clearly observed where adjacent faults interact. Cumulative displacements across these linkages would be considerably greater than the displacements attributed to individual faults. Note that the southern tips of faults 24 and 25 (image b) are obscured by coastal sediments.

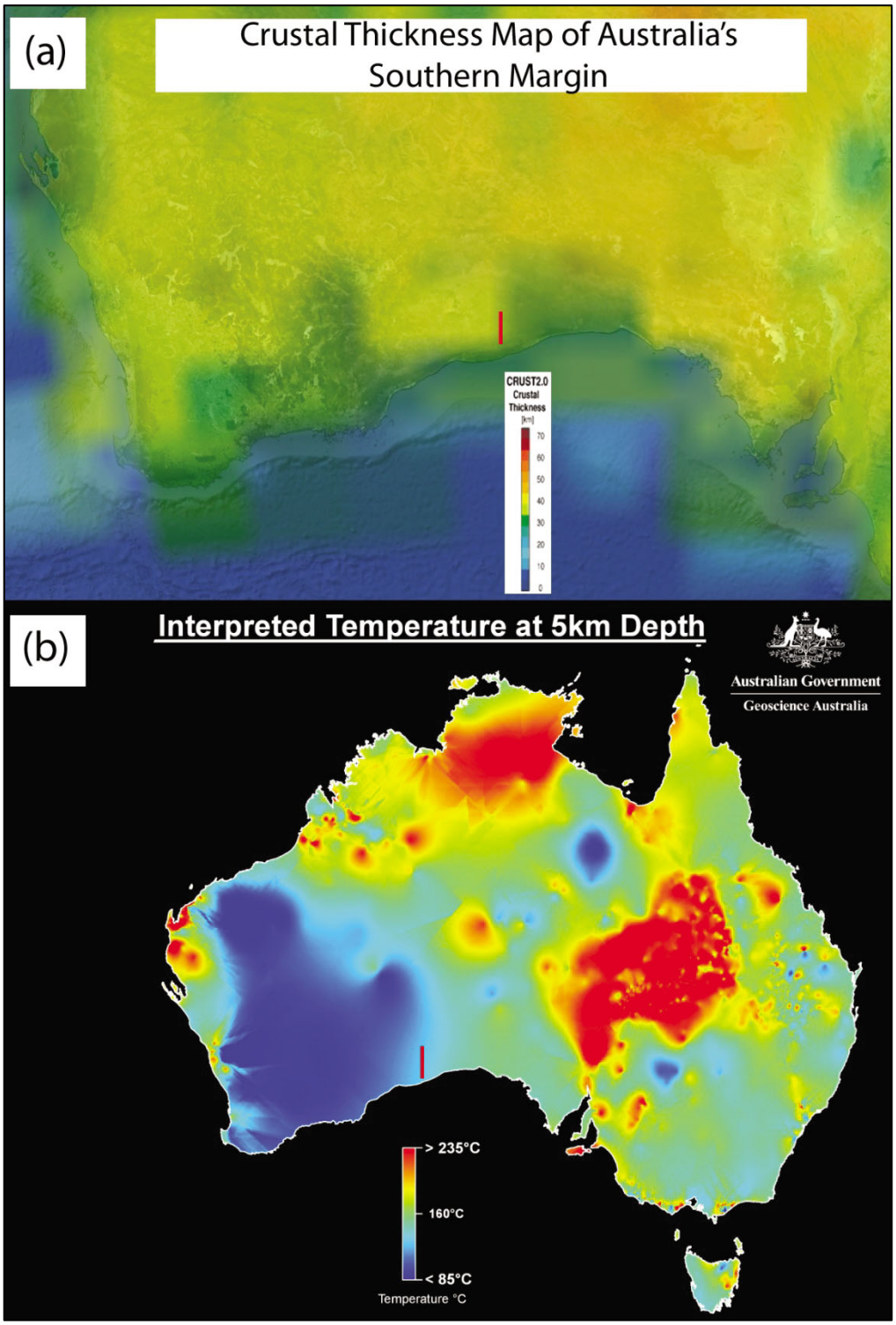

Figure 21: Maps depicting crustal thickness (a) and crustal temperature (b) each show a distinct boundary in their respective parameter that aligns with the position of the Mundrabilla Fault (delineated by a red line on each map). Crustal thickness map taken from Laske et al. (2013); temperature map adapted from Holgate and Gerner (2008).

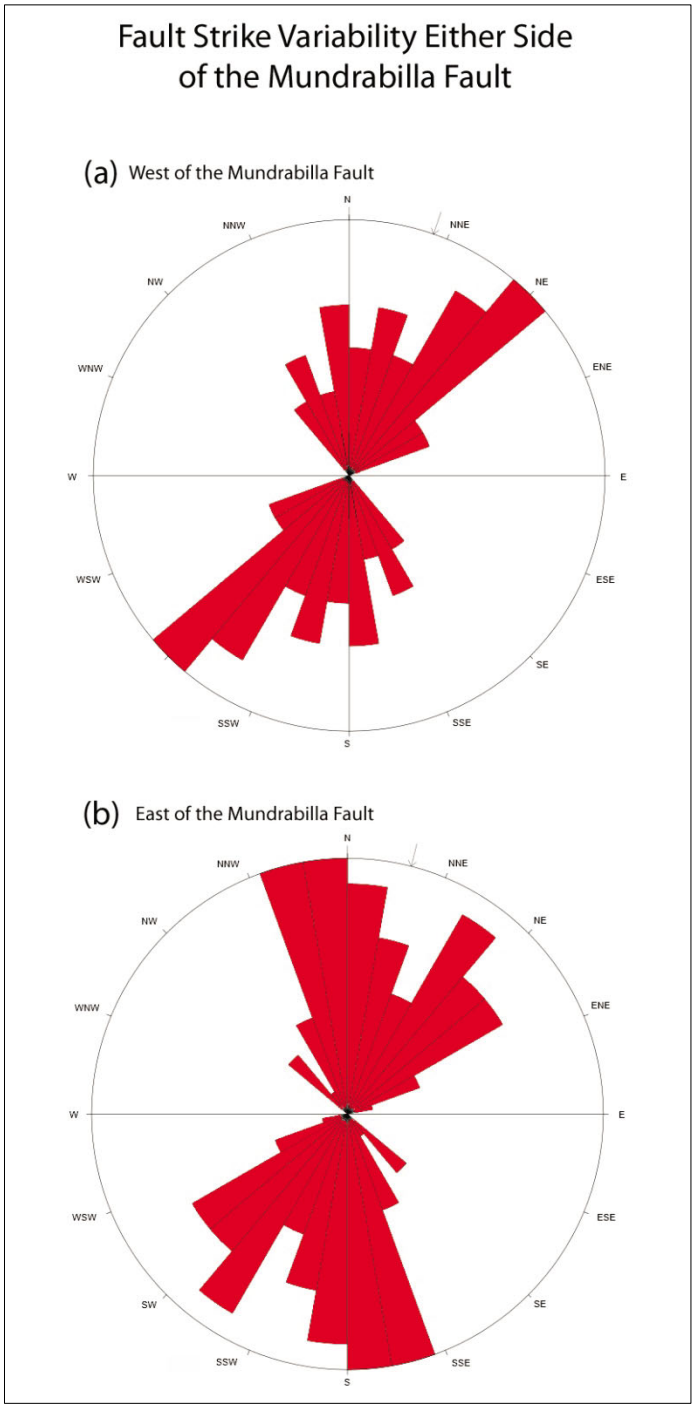

Figure 22: Rose diagrams depicting strike orientations for faults located to the west (a) and east (b) of the Mundrabilla Fault. Bin intervals are 10°. Faults to the west exhibited a mean strike value of 019 (based on 37 measurements of individual faults and discretely-oriented fault segments). Faults to the east of the Mundrabilla Fault (76 measurements in total) exhibited a mean strike orientation of 014. Whilst there appears to be a difference in modal strike intervals, the mean trend and total range of values recorded either side of the Mundrabilla Fault show little variability.

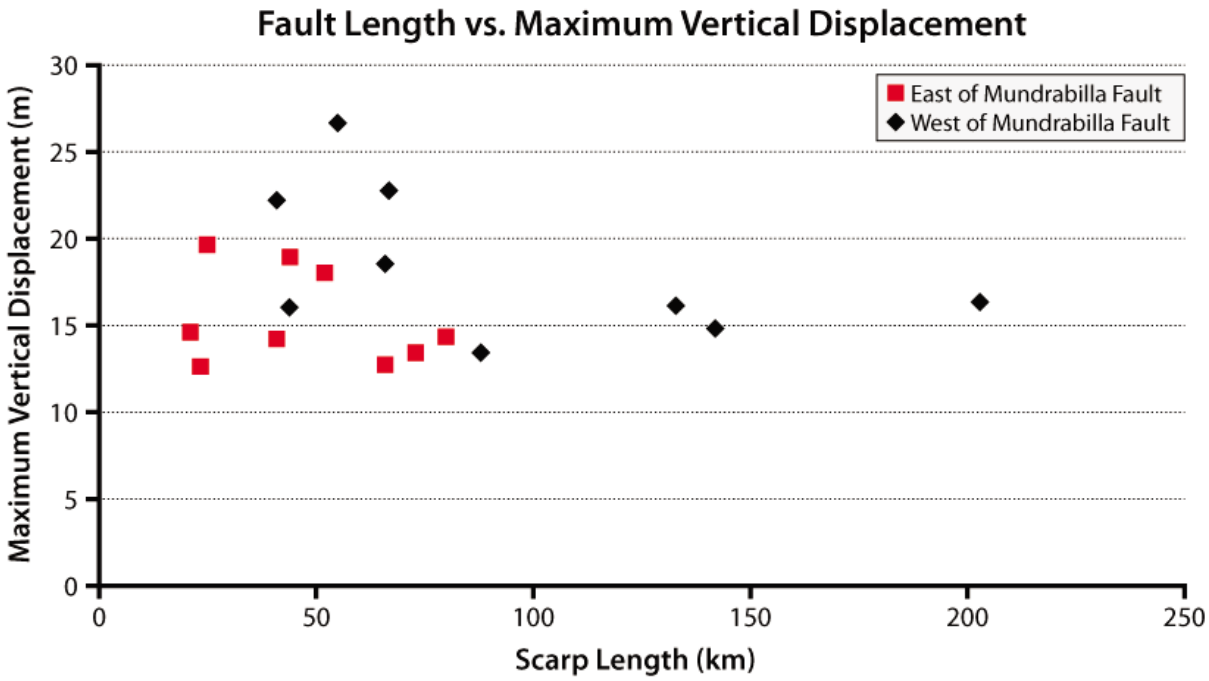

Figure 23: Fault growth patterns, as defined by 'displacement to scarp length' ratios do not appear to differ significantly for faults situated either side of the Mundrabilla Fault. Note, however, that the four longest fault scarps occur to the west of the Mundrabilla.

Note: As per figure 17, all faults that have been shown to continue beyond the study area have been eliminated from this analysis.

11.0 Tables

Table 1: Summary statistics for each of the 27 faults examined herein. Growth rates are calculated on the premise that the Nullarbor Plain faults are 15 million years old, and the Roe Plains faults are 2 million years old.

Fault #	Location	Scarp Length (km)	Max. Vertical Displacement (m)	Growth Rate (m/Ma)	Upthrown Side of Fault
1	Nullarbor Plain	133	16.1	1.1	E
2	Nullarbor Plain	203	16.3	1.1	E
3	Nullarbor Plain	88	13.4	0.9	E
4	Nullarbor Plain	142	14.8	1.0	W
5	Nullarbor Plain	41	22.2	1.5	W
6	Nullarbor Plain	55	26.6	1.8	W
7	Nullarbor Plain	67	22.7	1.5	E
8	Nullarbor Plain	66	18.5	1.2	W (northern segment); E (southern segment)
9	Nullarbor Plain	57	30.7	2.0	W
9	Roe Plain	50	13.4	6.7	W
10	Roe Plain	23	11.9	5.9	W
11	Nullarbor Plain	44	16.0	1.1	W
12	Nullarbor Plain	92	18.7	1.2	W
Mundrabilla	Nullarbor Plain	146	20.1	1.3	E
13	Nullarbor Plain	41	14.2	0.9	W
14	Nullarbor Plain	52	18.0	1.2	W
15	Nullarbor Plain	66	12.7	0.8	W
16	Nullarbor Plain	80	14.3	1.0	W
17	Nullarbor Plain	73	13.4	0.9	W
18	Nullarbor Plain	23.5	12.6	0.8	W
19	Nullarbor Plain	43	33.9	2.3	W
20	Nullarbor Plain	25	19.6	1.3	E
21	Nullarbor Plain	37	20.8	1.4	W
22	Nullarbor Plain	44	18.9	1.3	E
23	Nullarbor Plain	38	20.8	1.4	W
24	Nullarbor Plain	66	27.2	1.8	E
25	Nullarbor Plain	21.5	24.1	1.6	E
26	Nullarbor Plain	21	14.6	1.0	E

12.0 Appendices

Appendix 1: Methodology for the acquisition of lithostratigraphic contact elevations using a differential GPS and a total station:

Where a direct line of sight could be established between the differential GPS, the total station and the horizon of interest, a simple methodology could be employed. The differential GPS would be used to calculate the surface elevation at a specific point (effectively providing a known elevation benchmark). The total station would then be positioned at an intermediate point between the differential GPS and the contact of interest, such that the vertical distance to each could be measured by laser. The subtraction of each of these vertical distances from the known elevation benchmark would yield the elevation of the limestone horizon. Where the required line of sight could not be readily established, additional intermediate sighting points would be utilised as necessary. In extreme cases, where cave passages exhibited a high degree of tortuosity, the acquisition of accurate elevation data was deemed impossible.

Appendix 2 (part 1 of 6): A table detailing sedimentological data acquired in the field. Observations pertain to individual lithological units and contacts. Site coordinates are in GDA94. Units are coded as follows: Tmn = Nullarbor Limestone (Upper Member); Tmnm = Nullarbor Limestone (Mullamullang Member); Tma = Abrakurrie Limestone; Tew = Wilson Bluff Limestone; Roe = Roe Calcarenite.

Site	Latitude	Longitude	Tmn Sedimentology	Tmnm Sedimentology	Tma Sedimentology	Tew Sedimentology	Roe Sedimentology	Tmn / Tmnm Contact	Tmn / Tma Contact	Tmnm / Tma Contact	Tma / Tew Contact	Tma / Roe Contact	Other Notes
Capstan Cave	-32.016169	125.949791	Dominated by mouldic fossils; specifically bivalves, gastropods (mix of ornamented, squat and turreted varieties), LBF, rare oysters (original shell material preserved), uncommon echinoids and probable corals. Bivalves are present as singular and articulated valves. Fossil horizons define crude bedding planes.	Red rhodolith rudstone to floatstone with isolated gastropod and bivalve fossils.				Contact is defined by a slightly wavy but smooth bedding surface. Rhodoliths of the Mullamullang Member become smaller and less common within 30-50cm of the contact.					
Cocklebiddy Cave	-31.966592	125.9168498	Dominantly mudstone facies were encountered during the descent into the cave.		Well-sorted, pale, bioclastic bryozoan grainstone with isolated 'cm-scale' intraclasts and shell fragments. Contains coarser rudstone horizons with greater porosity and permeability. Notable pink discolouration in parts.	Chalky, white mudstone with floatstone horizons. Contains brachiopods (many of which are articulated) and ramose bryozoans.					Contact lies beneath a 40cm thick, tabular rhodolith floatstone-rudstone (with isolated gastropods, bivalves and corals) that defines the lowermost Abrakurrie Lst. A 30 cm-thick shelly horizon occurs immediately above the rhodolith floatstone-rudstone (containing gastropods, bivalves, echinoderm spines and bryozoans), which is overlain by more characteristic Abrakurrie Limestone.		Cross-laminations in the Abrakurrie Limestone: 071/14° SE.
Murra-el-elevyn Cave	-32.042777	126.038244			Echinoid horizons occur in Abrakurrie floatstones deeper in the cave. Bioturbation noted. Alternating massive floatstone-mudstone horizons and dense grainstone-rudstone levels.			Contact is defined by a decrease in the size and abundance of rhodoliths upward, followed by the development of a mouldic floatstone-rudstone. Finally, a bivalve-rich mouldic floatstone dominates (characteristic of the Nullarbor Limestone upper member).		Contact is defined by the appearance of bedding in the Abrakurrie Limestone and the disappearance of rhodoliths.			Large, single pecten bivalve noted in the upper Abrakurrie Limestone.
Dingo Cave	-31.853395	126.7344839	Not particularly fossiliferous, although the unit bears moulds of gastropods and bivalves.	Not particularly fossiliferous.				Contact is sharp here with rhodoliths disappearing abruptly (without a decrease in size). There is no obvious succession by a mouldic, bioclastic floatstone at the top of the bed (as seen elsewhere).		Void space along the Abrakurrie-Mullamullang Member contact is filled with horizontally laminated flowstones in areas. The Abrakurrie limestone is noticeably fossiliferous near the contact (it is a floatstone with rudstone pockets). Echinoids (mostly irregular) and bivalve fragments are common.			A high degree of weathering was noted during the descent into the cave- rough, vuggy surfaces and flowstones are present.

Appendix 2 continued (part 2 of 6)

Site	Latitude	Longitude	Tmn Sedimentology	Tmnm Sedimentology	Tma Sedimentology	Tew Sedimentology	Roe Sedimentology	Tmn / Tmnm Contact	Tmn / Tma Contact	Tmnm / Tma Contact	Tma / Tew Contact	Tma / Roe Contact	Other Notes
Firestick Cave	-31.769927	127.0277598						Contact is difficult to discern due to travertine-style calcite precipitation.		Contact is difficult to discern due to travertine-style calcite precipitation.			Planar bedding horizon noted in the Mullamullang Member just above the Abrakurrie - Mullamullang Member contact.
Mullamullang Cave	-31.723268	127.2297447	Mouldic bioclastic mudstones-floatstones, dominated by gastropods and bivalves. At the surface, the Nullarbor Limestone displays pronounced karst features.	Rhodolith floatstone-rudstone.	Contains cross-sections of whole echinoids and moulds of gastropods.			Contact is obscured by iron staining (it is dificult to define).		Sharp contact, well-defined across the cave wall (marked by a recessed cleft with a rhodolith rudstone-floatstone overlying an echinoderm-dominated floatstone. Contact is laterally uniform.			
Roaches Rest Cave	-31.556136	127.2373339	Notably fossiliferous horizons of mouldic, bioclastic floatstone (approaching rudstone in parts). Large gastropods dominate some horizons (up to 10cm in size and mostly complete) and bivalves dominate others. Many pectens appear to have retained original shell material whilst other bivalves and gastropods haven't. LBF are also present.										
Abrakurrie Cave	-31.657188	128.4892652	Contains cm-scale mudstone intraclasts, LBF, bivalves and gastropods. Surprisingly, also contains bryozoans and isolated echinoids at higher stratigraphic levels.	Thin unit with basal portions bearing rhodoliths up to a maximum of 3cm in diameter. Rhodoliths decrease in size and abundance upwards.	Bryozoan grainstone with common echinoid bioclasts- some brachiopods and bivalves are also present. Floatstone-rudstone facies. Where developed, bedding is typically tabular and laterally persistent. Bryozoan hash matrix becomes more clearly developed down-section. Large sheets of fenestrate bryozoans identified, reaching approximately 5cm in size.	Chalky and fossiliferous in nature. Echinoids, brachiopods and bryozoans are most common, but pectens and other bivalves are also present. Weakly-defined bedding is present in places (medium-thick). Unit is otherwise massive.		Contact is relatively well-defined by the disappearance of rhodoliths. Weakly developed parting plane at the contact.			Contact appears to be irregular in nature.		Joint face within the cave: 139° (vertical).
Kutawala Cave	-31.682286	128.4963439	Thickly (crudely) bedded pink-grey-brown mudstones and floatstones with rudstone intervals. Fossils are mostly mouldic, comprising disarticulated bivalves and gastropods. Fossils are commonly large and complete, although broken fragments are found within the calcisiltite matrix. Complete irregular echinoids found within the basal 2 metres. A 30cm-thick LBF-rich horizon lies approximately 1.15m above the Upper Member - Mullamullang Member contact.	Thin Mullamullang Member at this location identified by a dominance of rhodoliths, however, mouldic solitary corals, bivalves and gastropods were also present. Rhodoliths were relatively small (up to 4cm diameter).				Contact is defined by a distinct bedding plane (mouldic fossil horizon, below which the rhodoliths become smaller and isolated).		Contact is well expressed. Gentley undulating and relatively uniform over several metres. Karstic dissolution features evident on a local scale.			Massive limestone marks the top few metres of the exposure.

Appendix 2 continued (part 3 of 6)

Site	Latitude	Longitude	Tmn Sedimentology	Tmnm Sedimentology	Tma Sedimentology	Tew Sedimentology	Roe Sedimentology	Tmn / Tmnm Contact	Tmn / Tma Contact	Tmnm / Tma Contact	Tma / Tew Contact	Tma / Roe Contact	Other Notes
Weebubbie Cave	-31.654338	128.7752821	LBF are particularly large- up to 5cm in diameter. Unusual concentrations of echinoids also noted.						Contact difficult to identify due to the absence of the Mullamullang member. No defined unconformity is apparent. Contact was picked where fauna changed from a gastropod-bivalve-echinoid-LBF assemblage to an echinoid-brozoan assemblage.				Gastropod shell lags eveident in the Nullarbor Limestone upper member.
Winbirra Cave	-31.70618	128.5009956	Mouldic bivalves, gastropods and solitary corals. Small, red ooid/pisoid lime bodies are present on weathering faces.		Abundant echinoids and large, colonial bryozoans.				Contact tentatively identified based on fossil fauna. Brecciation and disturbance of beds is apparent near the contact.				Bedrock is intensely brecciated / fractured, reminiscent of fault breccia. Units are difficult to identify.
Eucla Pass	-31.675789	128.8799299	Mouldic bivalves (predominately single valves), gastropods, corals and LBF anre present. Pale pink colouration.		Rudstone dominated by large colonial bryozoans in a matrix of bryozoan-echinoderm hash. Large echinoids and isolated bivalves identified.			Excellent exposure of a sharp contact. Oysters are situated preferentially adjacent and parallel to the contact - possible hardground. Palaeokarstic depressions along the contact are filled with Nullarbor Limestone. Although the contact is sharp, no parting plane is recognisable.					
Wilson Bluff	-31.67552	129.0420396	Massive mudstones and floatstones of mouldic gastropods, bivalves, corals and LBF.			Chalky, white unit dominated by echinoids and brachiopods (also containing gastropods, bivalves and bryozoans).			Contact is not particularly well-defined. It was picked at the faunal change from a gastropod-bivalve-coral-LBF assemblage to an echinoderm-bryozoan assemblage.				
Najada East	-31.714362	128.6950007	A floatstone containing echinoid spines, LBF and bivalves (bed is appproximately 40cm thick).		Complete echinoids and colonial bryozoans set in a coarse bryozoan hash. Unusually, bivalves are common towards the top of the Abrakurrie Limestone. Iron-stained or mineralised horizons were noted above a distinct laminated / liesegang-banded section. Sub-horizontal to sub-vertical burrows up to 2cm in width were noted in the upper Abrakurrie Limestone.				The exact position of the contact was ambiguous (constrained to approximately 2m). The chosen contact marker is a sharp, well-defined boundary that is interpreted to be a hardground (bryozoa and echinoids common above and below the contact). Significant local relief along the contact.				Mullamullang rhodolith rudstone found as float atop the section

Appendix 2 continued (part 4 of 6)

Site	Latitude	Longitude	Tmn Sedimentology	Tmnm Sedimentology	Tma Sedimentology	Tew Sedimentology	Roe Sedimentology	Tmn / Tmnm Contact	Tmn / Tma Contact	Tmnm / Tma Contact	Tma / Tew Contact	Tma / Roe Contact	Other Notes
Najada Rockhole	-31.734013	128.5906193							Defined boundary identified approximately 1 m below the proposed Nullarbor - Abrakurrie Limestone contact, but echinoids and bryozoans were found above this hardground / palaeokarst. Contact was defined as the first appearance of Nullarbor Limestone fauna (mouldic gastropods, bivalves, etc.). Small, isolated rhodoliths were identified at the approximate level of the contact. Iron staining/mineralisation was also present around the contact.				Karstification made the confident identification of facies and contacts difficult.
Water Truck Blowhole	-31.690934	128.7865424	A particularly fossiliferous expression of the Nullarbor Limestone, dominated by small gastropods and isolated bivalves, corals and LBF. Wackestone-mudstone facies predominate.		Notably echinoderm-rich in parts, also bearing abundant bryozoans. Orange staining in parts.				Contact was defined by an iron-rich, oxidised horizon. Fossils (inc. mineralised shells) are concentrated within depressions in this horizon - possibly a re-exposed palaeokarst.				Extensively karstified-lithologies were difficult to identify.
Nuneeja Rockhole	-31.903092	127.0584842	Mouldic wackestones and mudstones (presumably of the Nullarbor Limestone) were found above the inferred Nullarbor-Mullamullang contact.	Rhodolith floatstones were identified. Rhodoliths decrease in size and abundance towards the upper contact.	The Abrakurrie Limestone was less fossiliferous than usual at this location. Large fenestrate and ramose bryozoans were still present immediately below the inferred Abrakurrie - Mullamullang contact on the eastern side of the gully. Classic echinoderm hash grainstone found lower in the section where rhodoliths drop out completely.			Contact was difficult to define on the eastern side of the gully. It was taken to be the highest occurrence of rhodoliths after scouting a wide area.		Three exposures of this contact were identified here, and found to be at notably different elevations (i.e. one contact in a central stream bed, and the other two on flanking ridges). The spread of contact elevations implied that strata was dipping locally at approximately 20° to the NNE.			Loose shelly fossils of the Roe Calcarenite were found in an old surficial quarry off the Eyre Highway in this location. Mulamullang Member was also abundant in the quarry float. Karstified surfaces and poor outcrop on the gully slopes made lithological identification extremely difficult. A major differential in contact elevations was identified- possible evidence of a fault offset in the gully or dipping strata.
Old Madura Pass	-31.895347	127.0262381		Rhodolith floatstone.	Bryozoan-rich floatstone-wackestone facies.			Contact placed at the last occurrence of rhodoliths (which get smaller and less abundant towards the top of the unit). A mouldic shelly lag of large bivalves, gastropods and corals marks the boundary.		Contact not visible, but confidently constrained to within 50cm.			Units appear to dip (difficult to measure, but approximately 055/12°NW).
Madura Cave	-31.984558	127.039538										No Roe Calcarenite lithified in situ here (only found loose as float).	Apparent Thalassinoides horizon identified approximately 2-3m below the cave surface.

Appendix 2 continued (part 5 of 6)

Site	Latitude	Longitude	Tmn Sedimentology	Tmnm Sedimentology	Tma Sedimentology	Tew Sedimentology	Roe Sedimentology	Tmn / Tmnm Contact	Tmn / Tma Contact	Tmnm / Tma Contact	Tma / Tew Contact	Tma / Roe Contact	Other Notes
Madura Quarry	-32.039685	127.0450628					Friable to moderately firm floatstone with large bioclasts. Diverse fauna-gastropods, bivalves and LBF are dominant. Many shells show evidence of predation.					Floor of the quarry believed to represent the Abrakurrie planation surface. The surface gently undulates across the quarry (but is largely planar). Root grooves cut across the surface in areas, seemingly indicating the extent to which roots could penetrate (through the Roe Calcarenite) before encountering strongly lithified material (Abrakurrie Limestone).	
Nurina Cave	-32.016297	127.0074954			Typical bryozoan grainstone identified lower in the section.							Abrakurrie Limestone at the contact is chalky-pale grey and largely devoid of macrofossils (somewhat akin to the Wilson Bluff). Portions of Roe Calcarenite are seemingly welded to the unconformable underlying contact. A hard surface boring (filled with Roe Calcarenite) was identified along the contact.	Abundant LBF weathering out of the Roe Calcarenite into the surrounding soil.
Moodini Rockhole	-32.115569	127.078692					Roe Calcarenite here is moderately firm and relatively indurated. Karstified surface weathers to a red-light grey colour. Karst not intensively developed. Mudstone to packstone/rudstone facies dominated by gastropod bioclasts (also contains bivalves and echinoids). Dark lithic grains are present in mudstone facies. Gastropods tend to be the turreted form, commonly displaying predatory borings. Most bioclasts are smaller than 1cm. Matrix is a shelly hash in coarser pockets.						
Kanidal Beach	-32.238585	126.159611				Portions of lithified beach rock are comparable to both the Wilson Bluff Limestone (brachiopods, echinoids) and the Abrakurrie Limestone (bryozoans, induration). However, other units containing abundant gastropods, bivalves and current bedding (cross-laminations up to 30cm and herringbone cross-lamination). Possibly an outcrop of the Toolinna Limestone. Primary preservation of shelly material is indicative of a relatively young geological unit.						Shelly lags and cobbly beach horizons (with rhizoliths and flowstones) identified in cliff and dunes. An inferred planation surface appears to dip dramatically to the west.

Appendix 2 continued (part 6 of 6)

Site	Latitude	Longitude	Tmn Sedimentology	Tmnm Sedimentology	Tma Sedimentology	Tew Sedimentology	Roe Sedimentology	Tmn / Tmnm Contact	Tmn / Tma Contact	Tmnm / Tma Contact	Tma / Tew Contact	Tma / Roe Contact	Other Notes
Fox Hole Cave	-32.034907	126.1875873		The basal Mullamullang Member here comprises pink rhodolith floatstones (rhodoliths are relatively small and quite sparse).	The uppermost Abrakurrie Limestone is a mottled pink-orange-brown echinoderm wackestone with isolated larger bioclasts (possibly bryozoans). Vuggy weathering pattern noted. In parts, the uppermost Abrakurrie Limestone is a fossiliferous floatstone with large gastropods, echinoids, bryozoans and bivalves. Classic Abrakurrie (bryozoan grainstone) not seen higher in the section, only near the base of the exposure.					Contact is well-defined by a cave overhang, with more massive Mullamullang units above. On a local scale, the contact is planar and approximately horizontal.			
Pannikin Plain Cave	-32.031015	126.1835064		Brown rhodolith floatstone with bioclastic echinoderm material.	Orange-brown echinoderm wackestone.			Contact is defined by a decrease in rhodolith abundance in the uppermost Mullamullang Member, followed by a mouldic bioclastic lag prior to a relatively pronounced bedding plane (taken to be the contact).		A seemingly irregular contact (only identifiable on freshly broken surfaces). Rhodoliths immediately above the contact are small, and the lowermost Mullamullang Member appears to be thickly bedded (massive further up).			

…

Appendix 3: An example of the manner in which trend lines were applied to the fault displacement profiles, so as to minimise the effects of karstification on fault offset estimates. Here, the raw displacement data for fault three (blue line) has been fitted with a trend line.

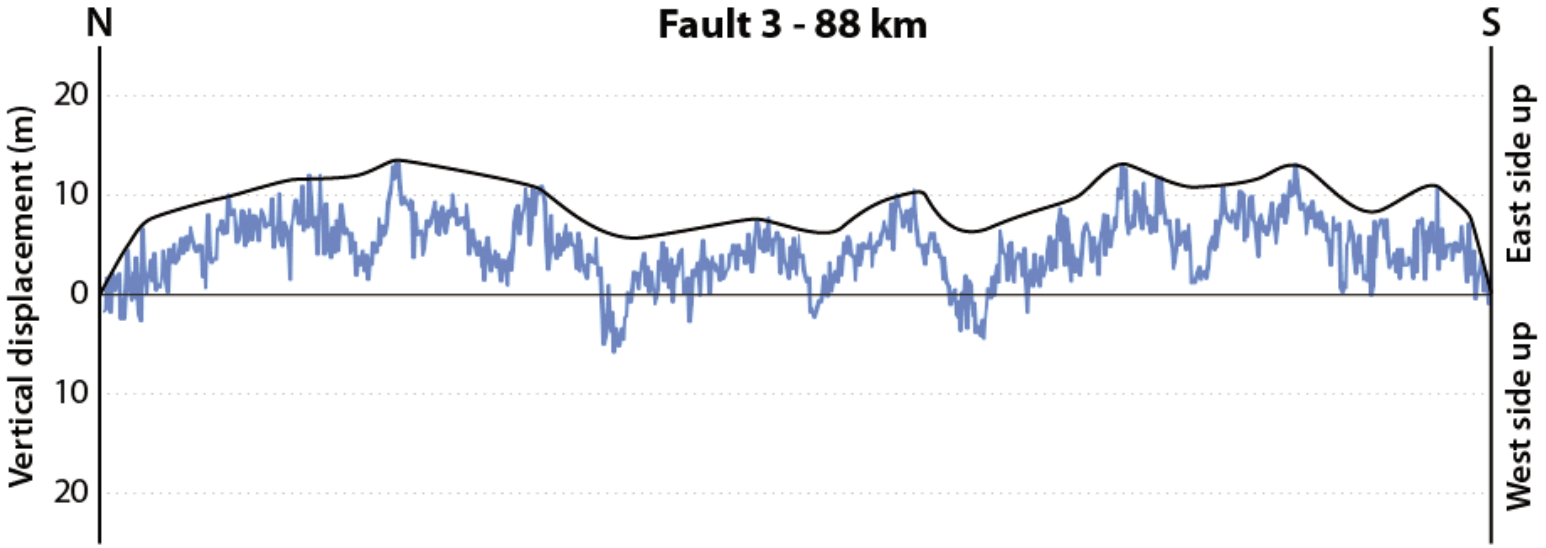

Appendix 4 (part 1 of 2): Table displaying the raw contact elevation data collected in the field. Elevations are referenced to mean sea level (Australian Height Datum). Site coordinates are GDA94. Lithological units are coded as follows: Tmn = Nullarbor Limestone (Upper Member); Tmnm = Nullarbor Limestone (Mullamullang Member); Tma = Abrakurrie Limestone; Tew = Wilson Bluff Limestone; Roe = Roe Calcarenite.

Site Name	Site Type	Latitude	Longitude	Base Tew	Top Tew	Tew Thickness	Base Tma	Top Tma	Tma Thickness	Base Tmnm	Top Tmnm	Tmnm Thickness	Base Tmn	Top Tmn	Tmn Thickness	Base Roe	Tew - Tmn Contact	Tew - Tma Contact	Tma - Tmnm Contact	Tmnm - Tmn Contact	Tma - Tmn Contact	Tma - Roe Contact
Capstan Cave	Field	-32.01616889	125.949791					65.200		65.200	71.906	6.710	71.906						65.200	71.906		
Cocklebiddy Cave	Field	-31.96659171	125.9168498		14.766		14.766	69.767	55.001	69.767	76.300	6.533	76.300	99.245	22.945			14.766	69.767	76.300		
Murra-el-elevyn Cave	Field	-32.042777	126.038244					63.305		63.305	73.425	10.120	73.425						63.305	73.425		
Dingo Cave	Field	-31.85339489	126.7344839					87.145		87.145	95.912	8.767	95.912	101.120	5.208				87.145	95.912		
Firestick Cave	Field	-31.76992681	127.0277598					80.504		80.504	90.985	10.481	90.985						80.504	90.985		
Madura Pass (Upper)	Field	-31.898776	127.009008					102.927		102.927									102.927			
Madura Pass (Lower)	Field	-31.898089	127.011222					94.241		94.241									94.241			
Mullamullang Cave	Field	-31.72326841	127.2297447					93.630		93.630	101.335	7.705	101.335						93.630	101.335		
Kestral Cavern No. 1	Field	-31.65732066	127.2193331					100.500		100.500	106.100	5.600	106.100	121.776	15.676				100.500	106.100		
Roaches Rest Cave	Field	-31.55613577	127.2373339					103.300		103.300	107.600	4.300	107.600	133.737	26.137				103.300	107.600		
Thylacine Hole	Field	-31.70777654	127.7367214					87.470		87.470	90.895	3.425	90.895	96.695	5.800				87.470	90.895		
Abrakurrie Cave	Field	-31.65718833	128.4892652		53.632		53.632	85.954	32.322	85.954	86.469	0.515	86.469	100.492	14.023			53.632	85.954	86.469		
Kutawala Cave	Field	-31.68228555	128.4963439					82.264		82.264	83.024	0.760	83.024	99.007	15.983				82.264	83.024		
Weebubbie Cave	Field	-31.65433848	128.7752821		45.200		45.200	75.478	30.278				75.478					45.200			75.478	
Winbirra Cave	Field	-31.70617999	128.5009956					83.624					83.624	95.821	12.197						83.624	
Eucla Pass	Field	-31.6757887	128.8799299					71.901					71.901								71.901	
Wilson Bluff	Field	-31.67552005	129.0420396		51.707		51.707	71.565	19.858				71.565					51.707			71.565	
Najada East	Field	-31.71436242	128.6950007					80.525					80.525	81.773	1.248						80.525	
Najada Rockhole	Field	-31.73401281	128.5906193					78.881					78.881	83.489	4.608						78.881	
Water Truck Blowhole	Field	-31.69093409	128.7865424					77.795					77.795								77.795	
Nuneeja Rockhole	Field	-31.90309177	127.0584842					83.010		83.010	104.312	21.302	104.312						83.010	104.312		
Old Madura Pass	Field	-31.89534692	127.0262381					69.066		69.066	78.767	9.701	78.767						69.066	78.767		
Madura Cave	Field	-31.98455774	127.039538					19.450								19.450						19.450
Madura Quarry	Field	-32.03968458	127.0450628					19.862								19.862						19.862
Nurina Cave	Field	-32.01629738	127.0074954					19.015								19.015						19.015
Kanidal Beach	Field	-32.23858463	126.159611		6.168																	
Fox Hole Cave	Field	-32.03490669	126.1875873					78.971		78.971	87.577	8.606							78.971			
Pannikin Plain Cave	Field	-32.03101511	126.1835064					75.516		75.516	84.115	8.599	84.115	88.416	4.301				75.516	84.115		
Trig Station NMF-228	Supplementary	-31.898056	127.04					81.30		81.30	93.80	12.50	93.80	107.50	13.70							
82NUR001	Supplementary	-30.031953	128.611776	175.00	187.50	12.50							187.50	196.00	8.50		187.50					
82NUR002	Supplementary	-30.020842	128.533855	175.00	187.00	12.00							187.00	193.00	6.00		187.00					
82NUR003	Supplementary	-30.009731	128.455936	153.00	174.00	21.00							174.00	178.00	4.00		174.00					
82NUR004	Supplementary	-30.181954	128.481913	159.00	172.00	13.00							193.00	197.00	4.00							
82NUR005	Supplementary	-30.19862	128.546845	165.00	171.00	6.00							171.00	200.00	29.00		171.00					
82NUR006	Supplementary	-30.1764	128.403991	153.00	175.00	22.00							175.00	193.00	18.00		175.00					
82NUR007	Supplementary	-30.331956	128.41698	128.00	162.00	34.00							168.00	175.00	7.00							
82NUR008	Supplementary	-30.40529	128.370226	132.00	168.00	36.00							168.00	174.00	6.00		168.00					
82NUR009	Supplementary	-30.498625	128.326072	120.00	166.00	46.00							168.00	175.00	7.00							
CD 1	Supplementary	-31.199102	129.351516	-44.00																		
CD 2	Supplementary	-31.167465	129.478461	-48.30																		
CD 3	Supplementary	-30.971402	129.279419	-8.00																		
BN 1	Supplementary	-31.1688454	129.1669693	-38.10																		
BN 2	Supplementary	-31.1624954	129.1635162	-39.10																		
KN 1	Supplementary	-31.3236406	129.7072923	-82.10																		
KN 2	Supplementary	-31.2272846	129.6535493	-52.00																		
Yangoonabie Bore (294)	Supplementary	-31.4673316	130.0721715	-81.73	48.72	130.45							48.72	67.62	18.90		48.72					
Cook Bore (295)	Supplementary	-30.6098844	130.4163782	57.00																		
Cook Bore 3 (298)	Supplementary	-30.6102473	130.4209952	55.00	87.00	32.00							87.00	125.00	38.00		87.00					
80EP 1	Supplementary	-31.314785	130.679198	-46.70	58.30	105.00							58.30	70.30	12.00		58.30					
80EP 2	Supplementary	-30.515604	130.5843815	74.70	90.70	16.00							90.70	120.70	30.00		90.70					
COOK 1 (370)	Supplementary	-30.8317518	130.6821251	-12.66	39.46	52.12							39.46	85.18	45.72		39.46					
Nullarbor Plains 2 (359)	Supplementary	-31.2621057	130.5869422	-70.87																		
Nullarbor Plains 5 (360)	Supplementary	-31.1570797	130.8943601	-14.68	40.30	54.98							40.30	85.90	45.60		40.30					

Appendix 4 continued (part 2 of 2)

Site Name	Site Type	Latitude	Longitude	Base Tew	Top Tew	Tew Thickness	Base Tma	Top Tma	Tma Thickness	Base Tmnm	Top Tmnm	Tmnm Thickness	Base Tmn	Top Tmn	Tmn Thickness	Base Roe	Tew - Tmn Contact	Tew - Tma Contact	Tma - Tmnm Contact	Tmnm - Tmn Contact	Tma - Tmn Contact	Tma - Roe Contact
Nullarbor Plains 6 (436)	Supplementary	-31.1490595	131.1938164	-26.39	37.62	64.01							37.62	68.10	30.48		37.62					
Roberts Well	Supplementary	-31.4446817	130.8858563	-66.49																		
EHBS 25	Supplementary	-31.4501453	130.9248751		21.00								21.00	56.00	35.00		21.00					
EHBS 25B	Supplementary	-31.444639	130.931078		23.80								23.80	56.80	33.00		23.80					
EHBS 24A	Supplementary	-31.372181	131.1811668		19.00								19.00	52.00	33.00		19.00					
Jubilee White Well Bore	Supplementary	-31.4322383	131.0042192	-66.87																		
YL 2	Supplementary	-30.2676551	131.1006408										78.80	104.80	26.00							
YL 3	Supplementary	-30.5274424	131.1279581	59.70	89.70	30.00							89.70	115.70	26.00		89.70					
ORP 2	Supplementary	-30.4518624	131.5570284										84.30	113.30	29.00							
Ooldea 1	Supplementary	-30.4601313	131.6301077										69.70	96.80	27.10							
Ooldea 2	Supplementary	-30.5857258	131.7597451										103.70	106.20	2.50							
Ooldea 3	Supplementary	-30.6288863	131.9159686										87.10	103.10	16.00							
PDH 1	Supplementary	-30.5196615	131.9744477										111.00	122.00	11.00							
PDH 2A	Supplementary	-30.512314	131.7336137										76.90	96.90	20.00							
PDH 3	Supplementary	-30.6035693	131.851903	94.20	98.20	4.00							98.20	110.20	12.00		98.20					
PIN-R 18	Supplementary	-30.616421	131.8825189										93.10	110.60	17.50							
PIN-R 33	Supplementary	-30.6311234	131.9507405										72.30	92.30	20.00							
PIN-R 20	Supplementary	-30.6708206	131.949861										58.50	84.50	26.00							
PIN-R 34	Supplementary	-30.6554481	131.9911155										68.00	90.00	22.00							
PIN-R 32	Supplementary	-30.5528612	132.0210278										90.00	111.00	21.00							
PIN-R 31	Supplementary	-30.6323532	132.0665645										98.70	100.70	2.00							
367 6 (131231)	Supplementary	-30.846134	132.1091981										90.00	96.10	6.10							
365 3 (131253)	Supplementary	-31.0431866	132.2540746										89.91	97.53	7.62							
602 4 (130921)	Supplementary	-31.2846588	132.3731079										41.20	43.20	2.00							
PIN-R 62	Supplementary	-31.3019679	132.5648395										38.00	39.00	1.00							
602 49 (130944)	Supplementary	-31.4635352	132.6195883										32.00	38.00	6.00							
602 2 (130919)	Supplementary	-31.2466472	132.4109011										43.90	48.90	5.00							
602 6 (131778)	Supplementary	-31.2844639	132.4529232										39.50	40.50	1.00							
602 46 (131266)	Supplementary	-31.4620895	132.4965224										36.50	41.00	4.50							
PIN-R 74	Supplementary	-31.5877611	132.6069512										41.30	44.30	3.00							
Tallacootra 2	Supplementary	-31.245293	132.3354437										47.10	54.10	7.00							
602 33 (130939)	Supplementary	-31.4271546	132.373346										38.50	43.00	4.50							
NDR 15	Supplementary	-31.8684945	132.2685114	16.00	22.00	6.00							22.00	33.00	11.00		22.00					
FW94 4	Supplementary	-31.5212924	132.1659102										32.00	50.00	18.00							
316-R 8	Supplementary	-31.337757	132.597543										38.95	41.39	2.44							
NDR 14	Supplementary	-31.9126831	132.3300335	-5.00	-1.00	4.00																
ODH 3A	Supplementary	-31.1828581	131.6247352	18.90	54.90	36.00							54.90	74.90	20.00		54.90					
ODH 13A	Supplementary	-30.8727	131.62042	33.00	56.00	23.00							56.00	75.00	19.00		56.00					
PIN-R 7	Supplementary	-30.8793894	131.8987334										47.10	71.30	24.20							
PIN-R 1	Supplementary	-31.0134716	132.051804										60.90	74.60	13.70							
Colona 1	Supplementary	-31.2725641	132.1445568										46.76	60.48	13.72							
TW 8	Supplementary	-31.1075596	131.9141365										36.00	63.00	27.00							
602 12	Supplementary	-31.3194543	132.536023										37.00	43.00	6.00							
COL 36	Supplementary	-31.4718806	131.7492073		7.40								7.40	46.90	39.50		7.40					
EHBS 12 - Highways	Supplementary	-31.6129818	131.9994601										-5.90	44.40	50.30							
NDR 11	Supplementary	-31.6439451	132.0771068	-20.00	14.00	34.00							14.00	30.00	16.00		14.00					
NDR 8	Supplementary	-31.7273997	132.1601543	6.00	10.00	4.00							10.00	32.00	22.00		10.00					
NDR 13	Supplementary	-31.6283392	132.0651177	-19.00	20.00	39.00							20.00	33.00	13.00		20.00					
FOR004	Supplementary	-31.28008	128.55396	-64.20	98.60	162.80							98.60	133.10	34.50		98.60					
FOR011	Supplementary	-30.61716	128.17583	102.10	158.10	56.00							158.10	178.10	20.00		158.10					
MAD014	Supplementary	-30.47861	127.08571	129.00	190.50	61.50							190.50	212.00	21.50		190.50					

RECORD 2016/10

EVOLUTION AND DEFORMATION OF THE ONSHORE EUCLA BASIN DURING THE CENOZOIC

Mounsher

This Record is published in digital format (PDF) and is available as a free download from the DMP website at <www.dmp.wa.gov.au/GSWApublications>.

Further details of geological products produced by the Geological Survey of Western Australia can be obtained by contacting:

Information Centre
Department of Mines and Petroleum
100 Plain Street
EAST PERTH WESTERN AUSTRALIA 6004
Phone: +61 8 9222 3459 Fax: +61 8 9222 3444
www.dmp.wa.gov.au/GSWApublications